Ultrahigh-Energy Cosmic Rays (UHECRs)
—observation, composition, and propagation—
Science 357, 1266 (2017) and other papers

Pierre Auger Observatory

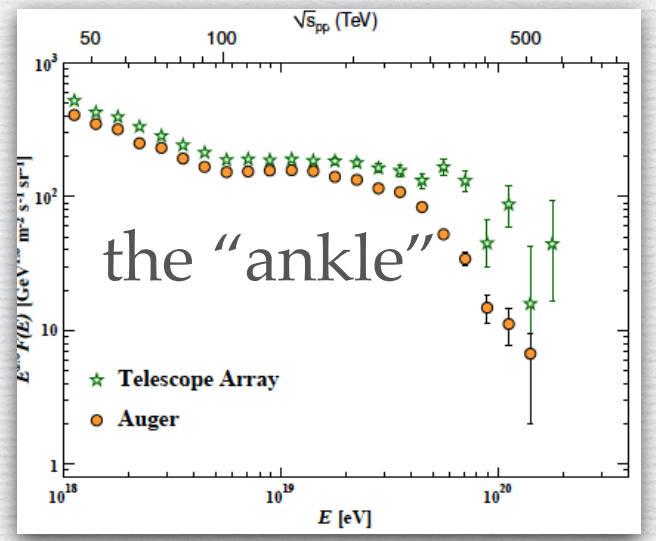

anisotropy

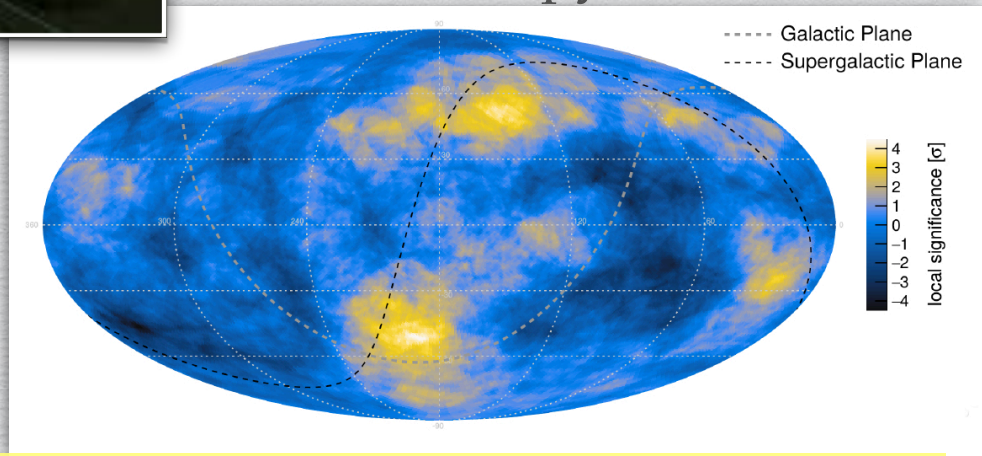

Extragalactic propagation

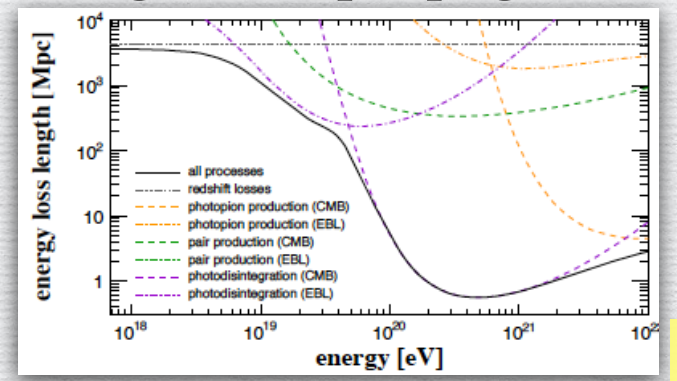

RCNP核理1aグループ勉強会 2019.7.18 by A. Tamii

Outline

I. Ultra-high-energy Cosmic Rays (UHECRs)

II. Observatories

III. Analysis Methods

IV. Composition

V. Energy Loss Process in Space Propagation

VI. Anisotropy

VII. (Acceleration Mechanism)

VIII. (Future Prospects)

Motivation on selecting this topic

We have started **PANDORA project** as a joint project among three experimental facilities **RCNP/ iThemba LABS/ELI-NP** for the study of energy-loss (photo-disintegration) process of UHECR nuclei in the extragalactic propagation.

UHECRs

Primary Cosmic Ray Flux and Composition

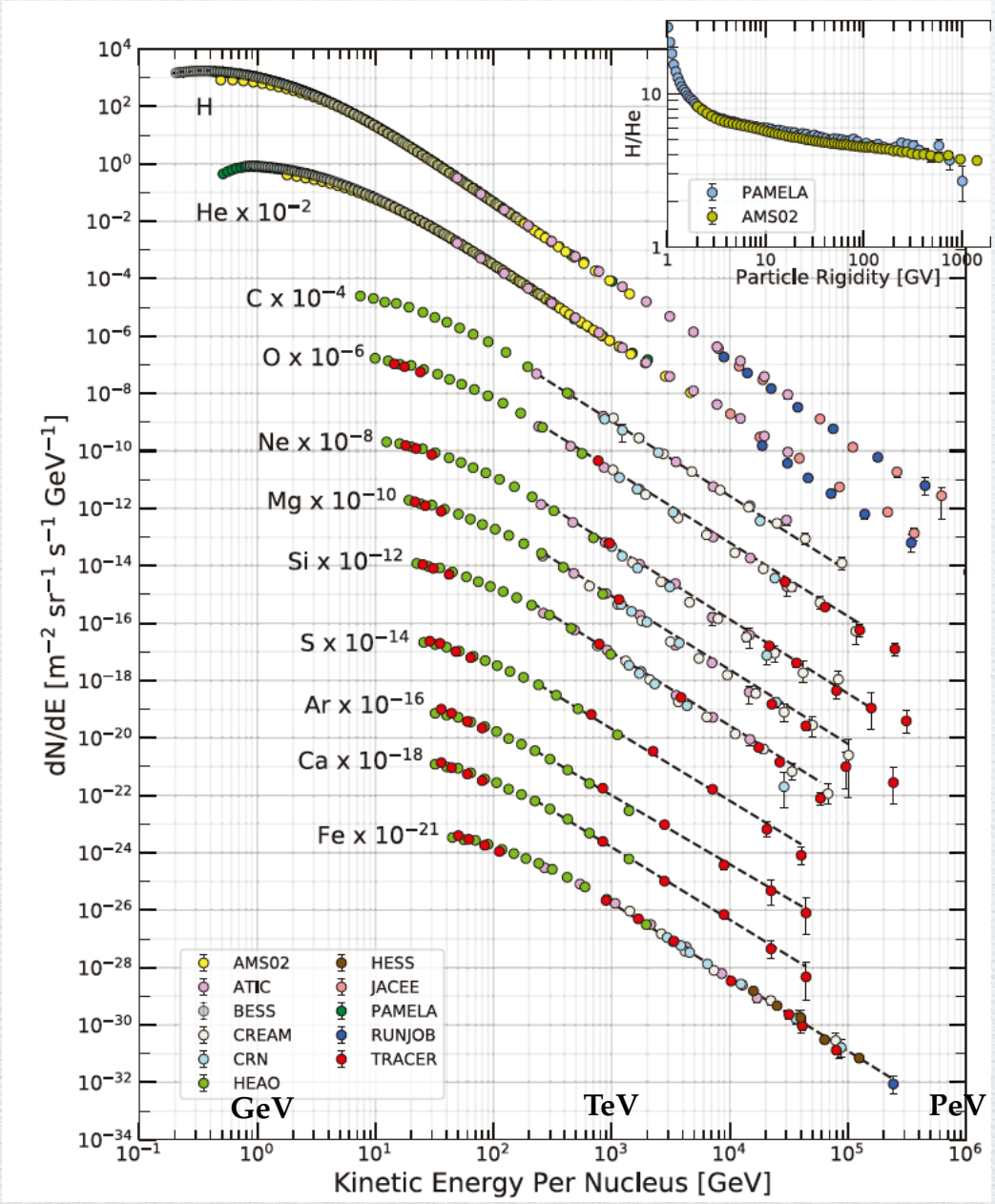

Z	Element	F	Z	Element	F
1	H	550	13–14	Al-Si	0.19
2	He	34	15–16	P-S	0.03
3–5	Li-B	0.40	17–18	Cl-Ar	0.01
6–8	C-O	2.20	19–20	K-Ca	0.02
9–10	F-Ne	0.30	21–25	Sc-Mn	0.05
11–12	Na-Mg	0.22	26–28	Fe-Ni	0.12

composition relative to oxygen at 10.6 GeV/A

[PDG2018]

Ultra-High-Energy Cosmic Rays (UHECRs) [PDG2018]

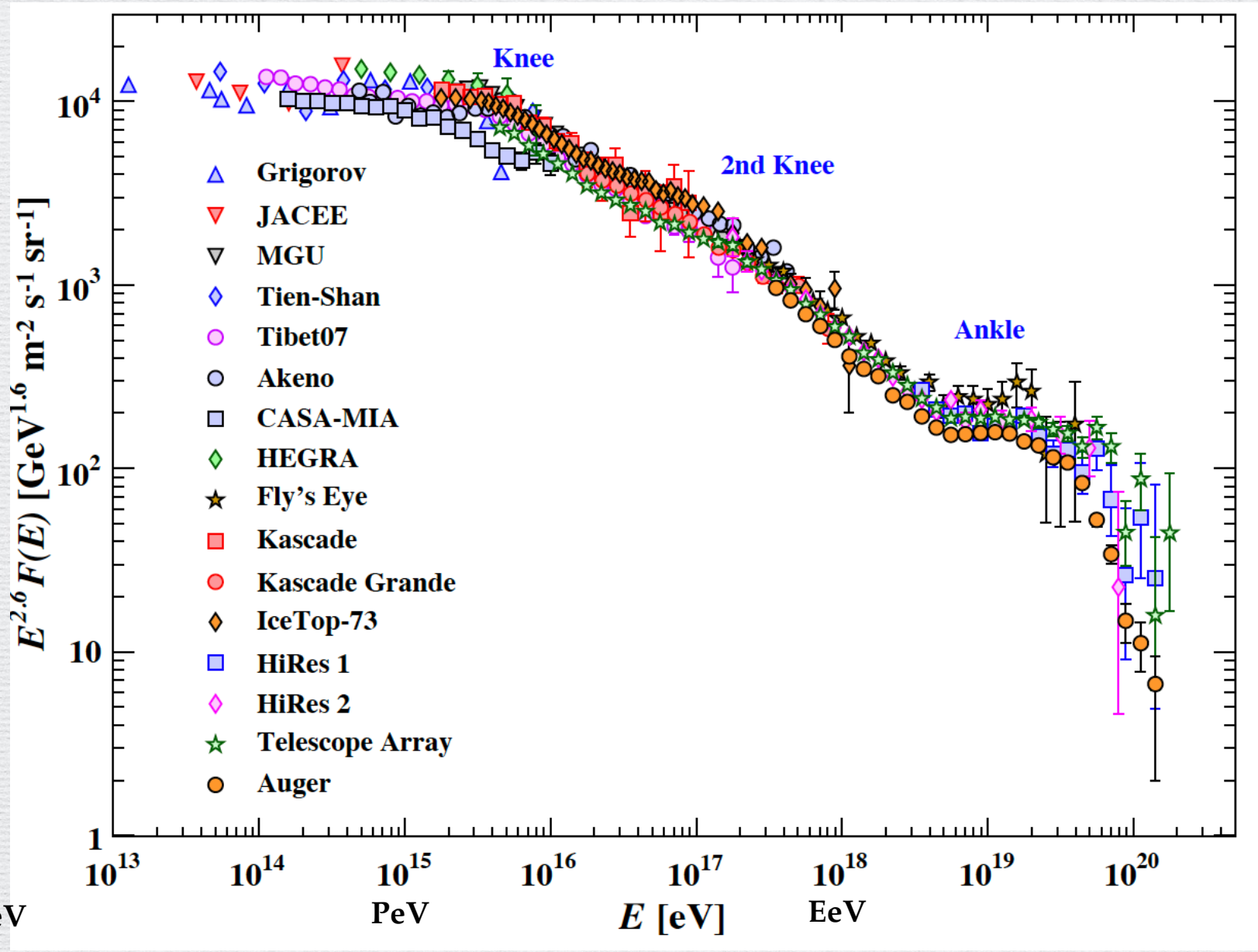

Ultra-High-Energy Cosmic Rays (UHECRs) [PDG2018]

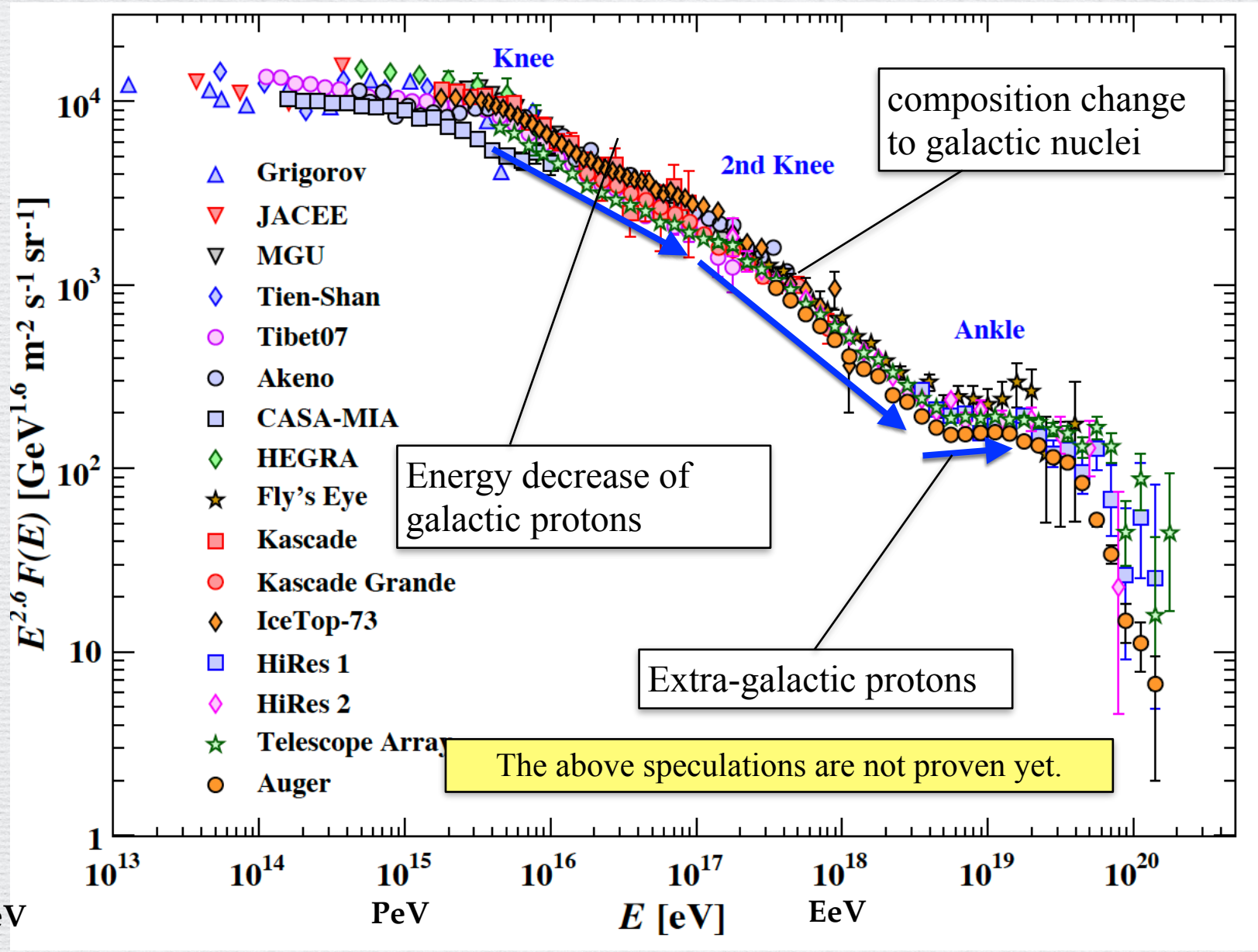

Ultra-High-Energy Cosmic Rays (UHECRs)

[anc19]

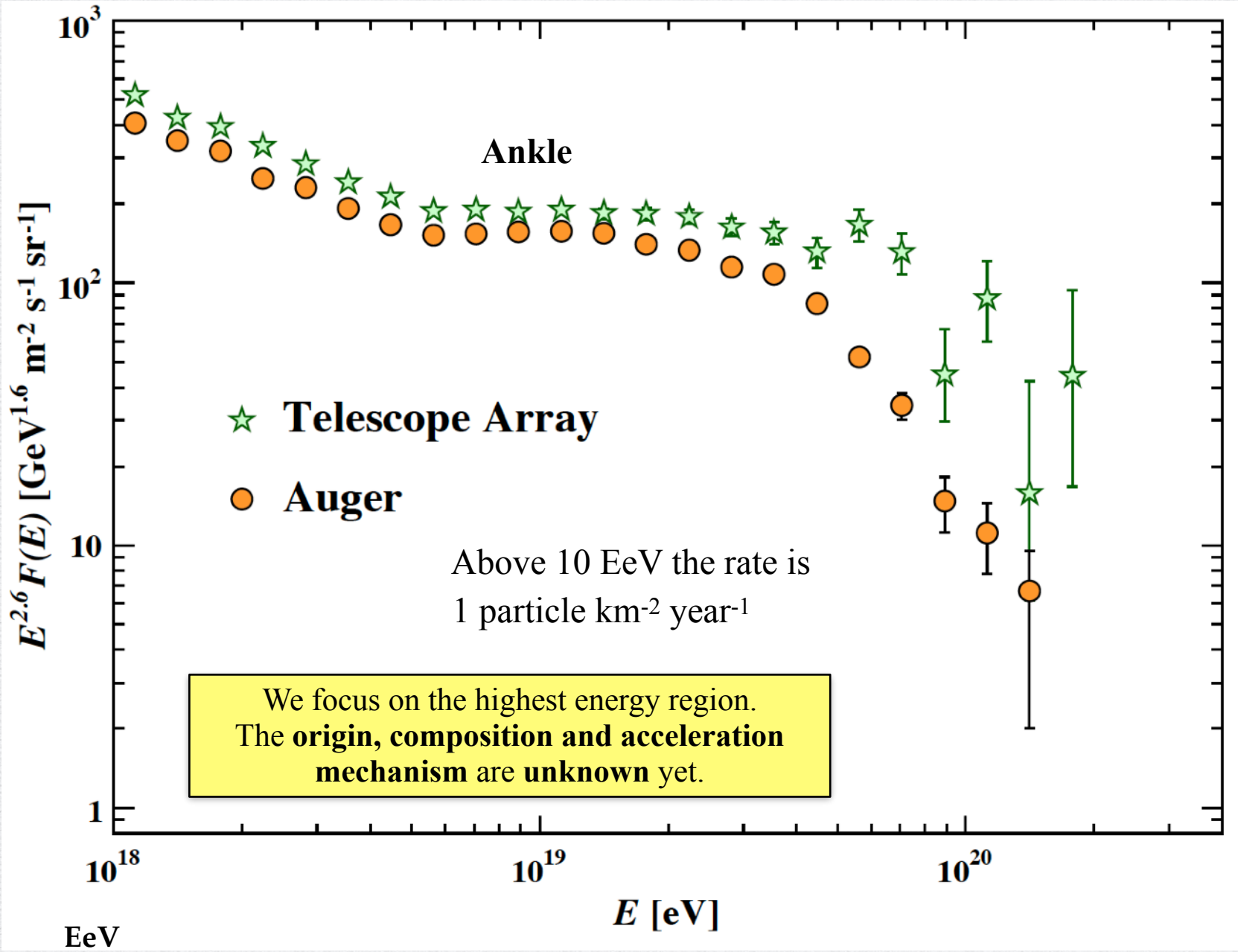

UHECR Observatories

Observation of UHECRs

Extended Air Shower (EAS)

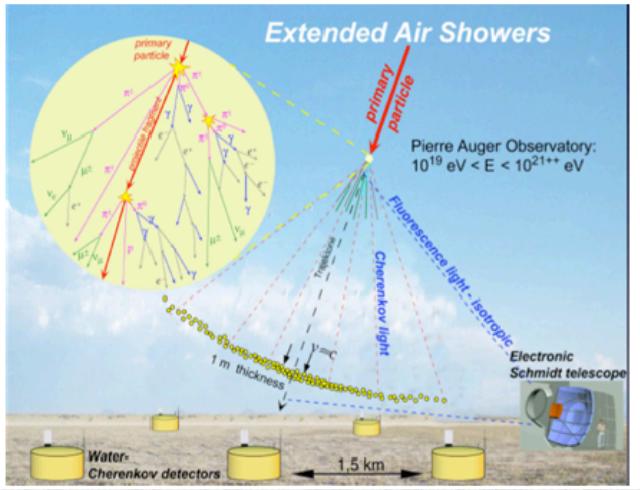

Hadronic process

primarily produces mesons (π or K)

p(A) +A $\rightarrow$ π, K, and nuclear fragments

$\pi^{\pm} \rightarrow \mu^{\pm} + \nu_{\mu}$ ($\overline{\nu}_{\mu}$)

$\pi^0 \rightarrow 2\gamma$

$\gamma \rightarrow e^+ + e^-$

$e^{\pm} + A \rightarrow e^{\pm} + A + \gamma$

Electromagnetic Shower

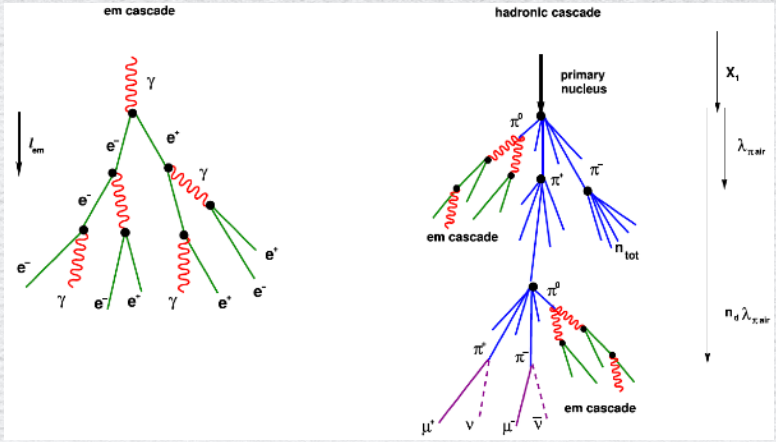

[mol18]

Pierre Auger Observatory

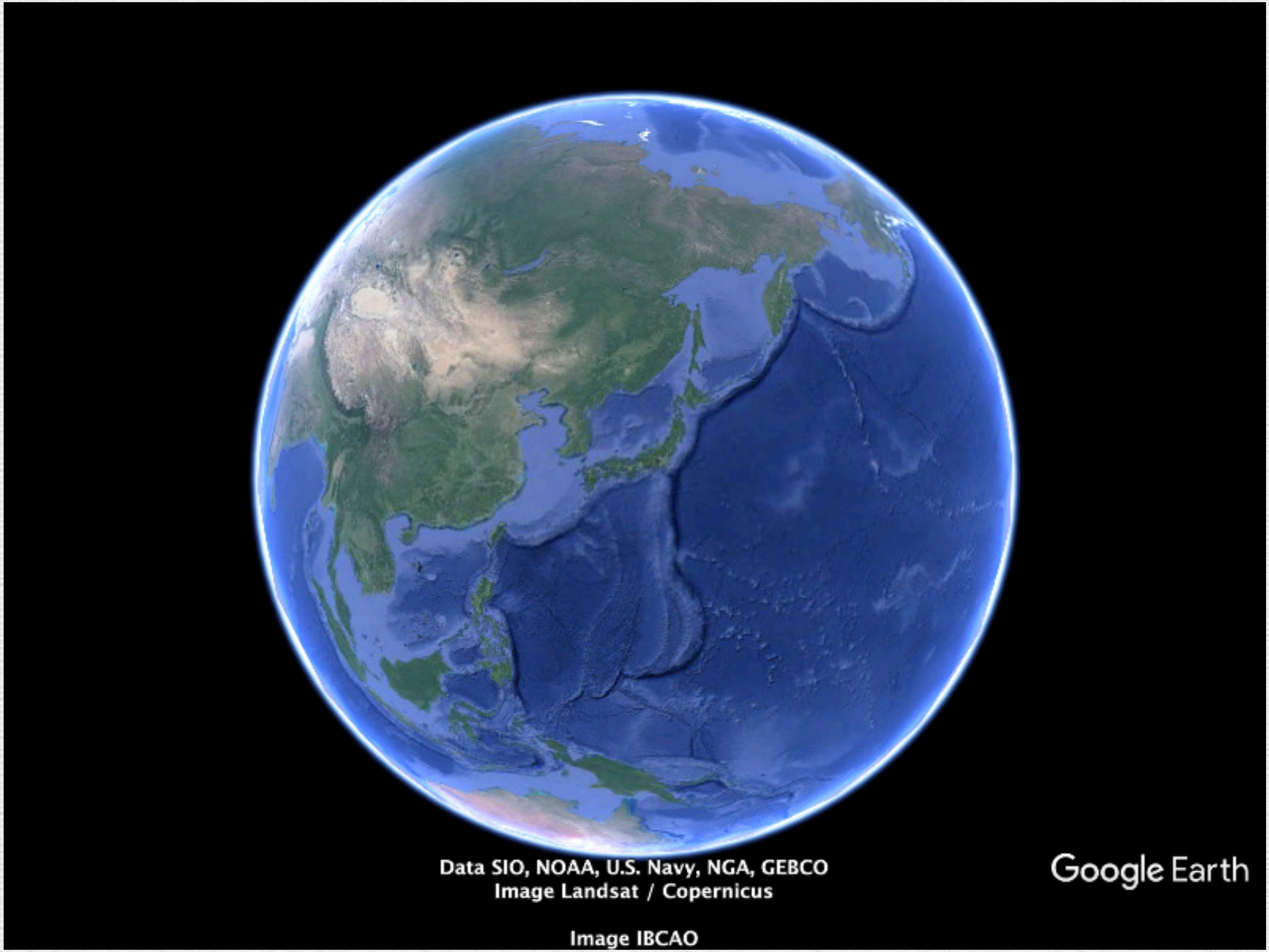

Pierre Auger Observatory

[aug15, aug04]

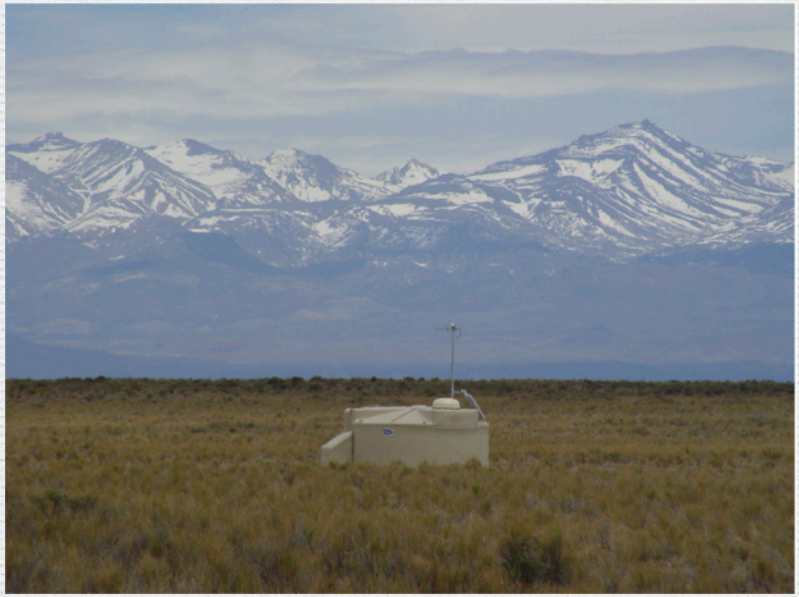

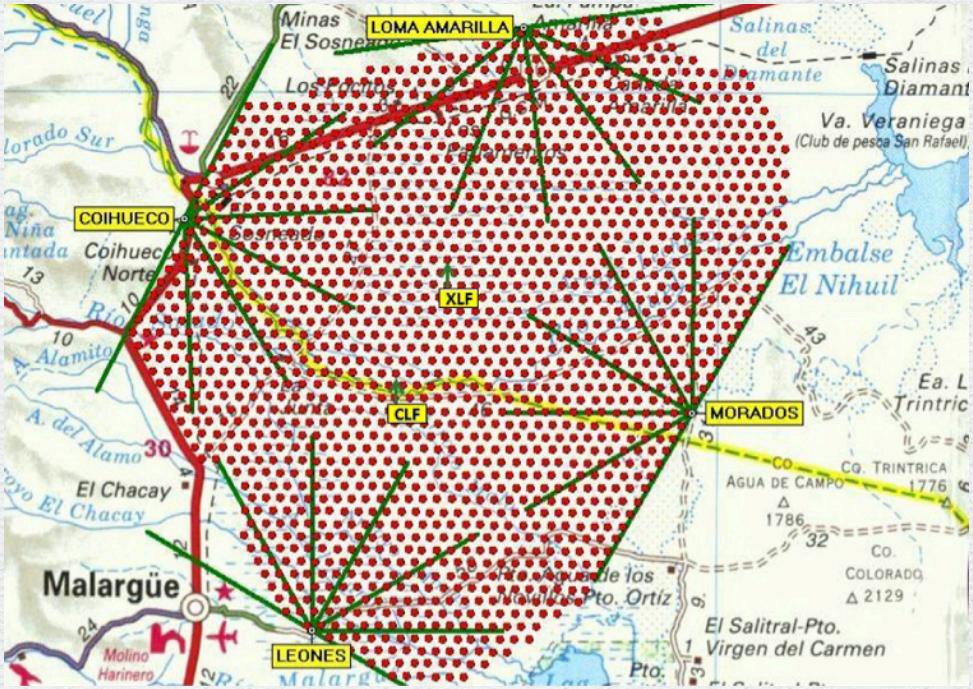

The Pampa Amarilla site (35.1°–35.5° S, 69.0°–69.6° W and 1300–1400 m asl) lies in the south of the Province of Mendoza, Argentina, close to Malargüe (pop. 18 000) and 180 km south west of San Rafael (pop. 100 000). It encompasses an area of 3100 km^2 (see Fig. 1a).

Pierre Auger Observatory

©google map

Pierre Auger Observatory

©google map

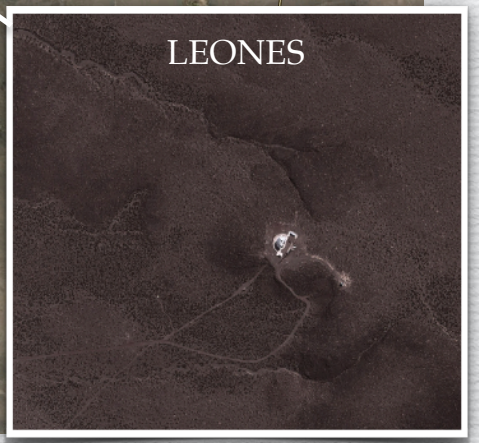

Pierre Auger Observatory
Surface Detector (SD)

[aug04]

3,000 km² (~60kmϕ)

1,600 water Cherenkov detectors (SD)
in a polyethylene tank

mean distance 1.5 km on triangular grid

~0.5 SD / km²

High-purity water
in three-layers of polyolefin liner
(140+28+178μm)

10 m² area × 1.2 m depth

Three PMT's

Hamamatsu R5921 8″ϕ
or
Photonis XP1802 9″ϕ

FADC 40 MHz

Time recording calibrated by GPS.
(σ=7.24 ns)

100% running efficiency measured from 2004

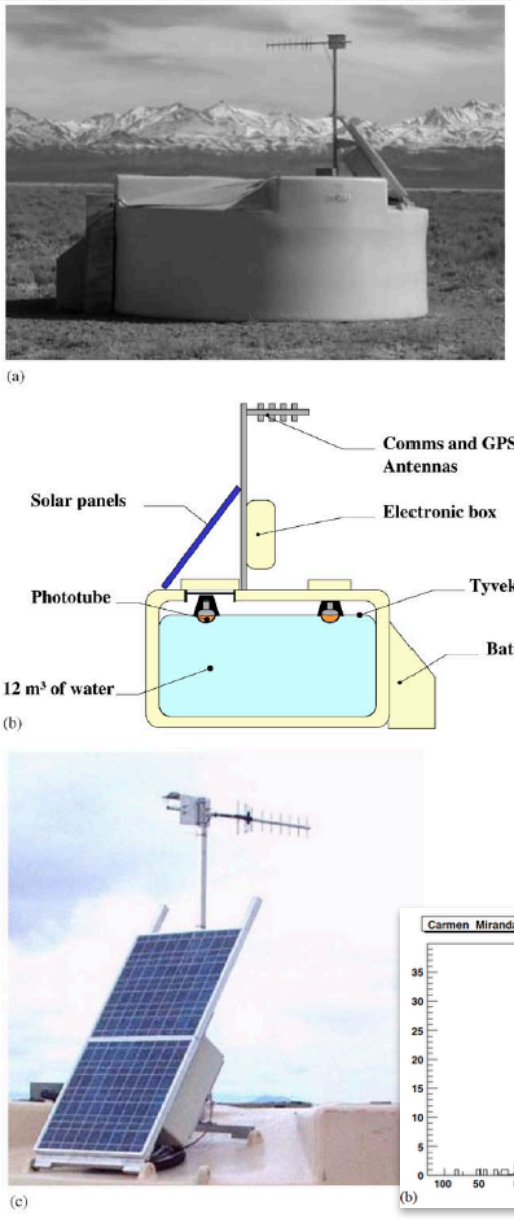

Fig. 2. (a) A photograph of an EA water tank; (b) schematic view of an EA tank; (c) the Yagi antenna and the solar power array.

Pierre Auger Observatory
Surface Detector (SD)

Areal coverage = 1600×10 m^2 / 3000 km^2 = $\sim 5 \times 10^{-6}$

Above 10 EeV

→ 10^{10} particles / 20 km^2

→ 2×10^3 particles penetrates 10 SD

1 particles km^{-2} year^{-1}

Pierre Auger Observatory
(Fluorescence Detector) FD

[aug15, aug04]

24 fluorescence detector telescopes at 4 sites

with spherical mirror (3.5m×3.5m)
and (440) PMT camera

30° azimuth×28.6° elevation field of view per telescope

UV light 310-390 nm
fluorescence from nitrogen in the air

Continuous digitization by 10MHz 12 bit ADC

100 Hz recording using sum trigger and threshold (20μsec)

Calibrated by YAG-laser (355nm) from CLF and XLF

~15% running efficiency with clear sky no moon

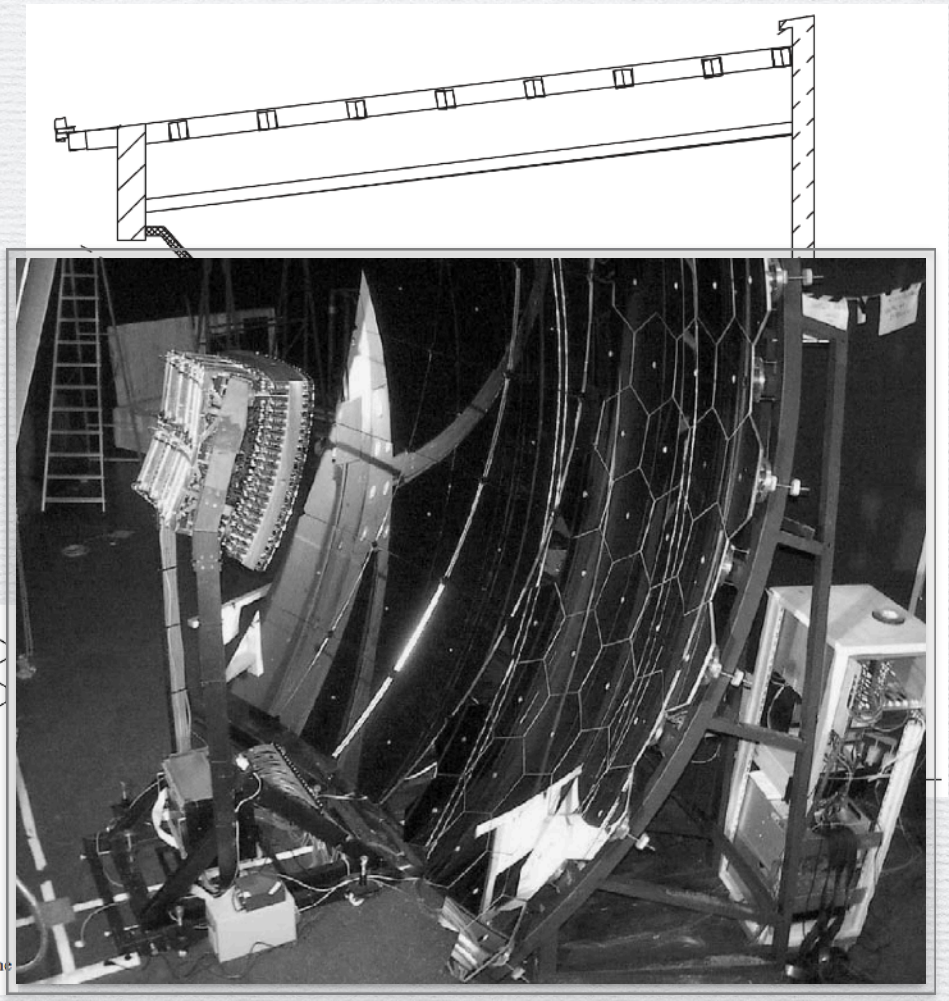

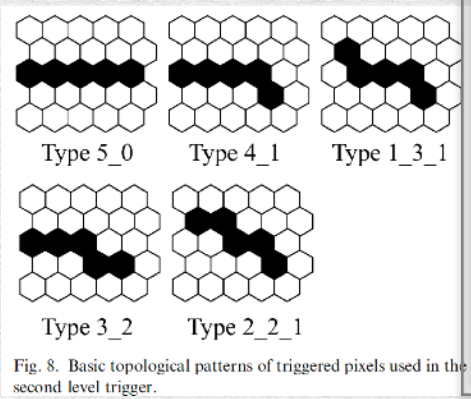

Fig. 8. Basic topological patterns of triggered pixels used in the second level trigger.

Telescope Array

Telescope Array

[tok11, abu12,]

The TA site is located in the desert about 1400 m above sea level centered at 39.3°N and 112.9°W in Millard County, Utah, USA, about 200 km southwest of Salt Lake City. A control center to support

Telescope Array

[tok11, abu12,]

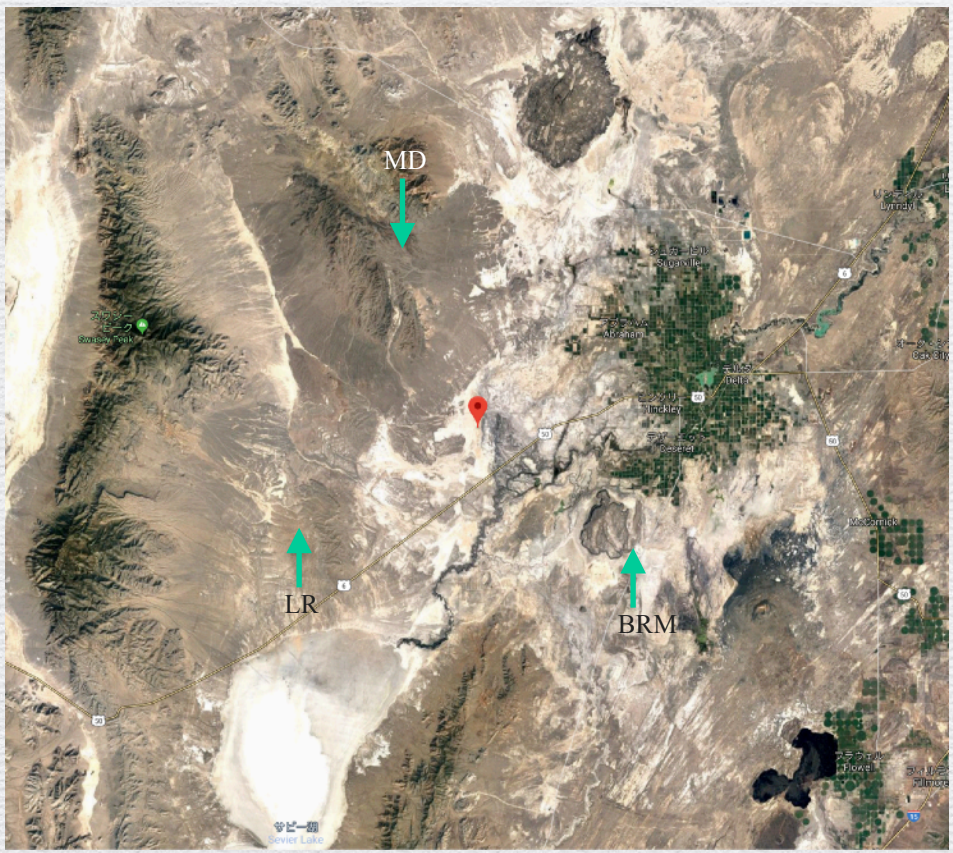

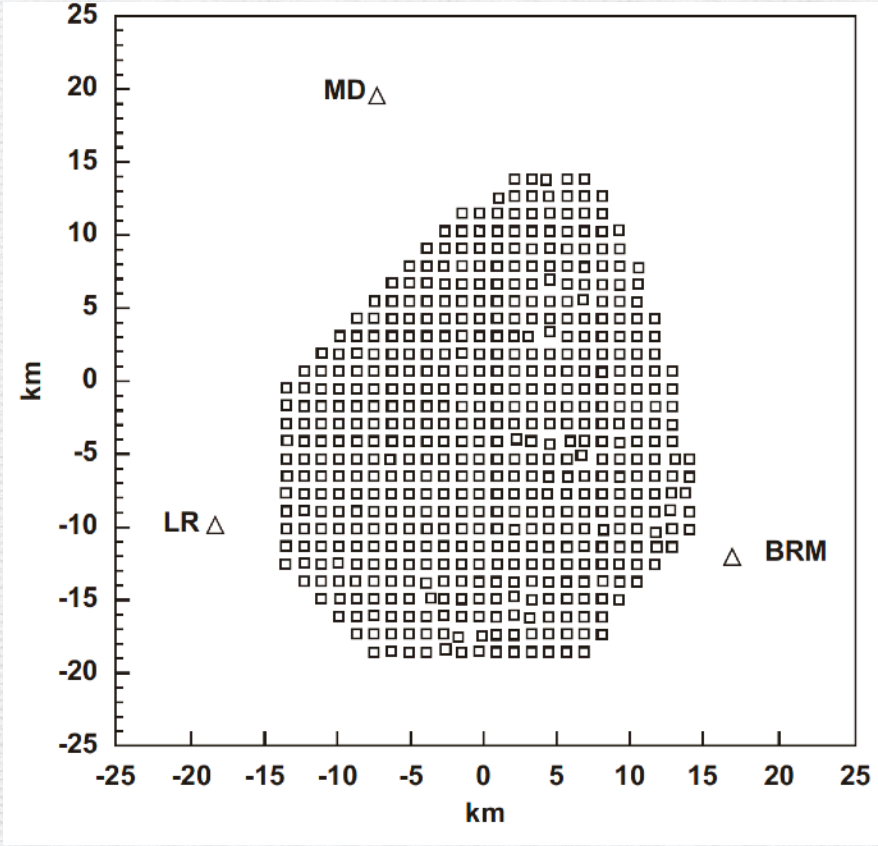

The TA site is located in the desert about 1400 m above sea level centered at 39.3°N and 112.9°W in Millard County, Utah, USA, about 200 km southwest of Salt Lake City. A control center to support

Telescope Array

[tok11, abu12,]

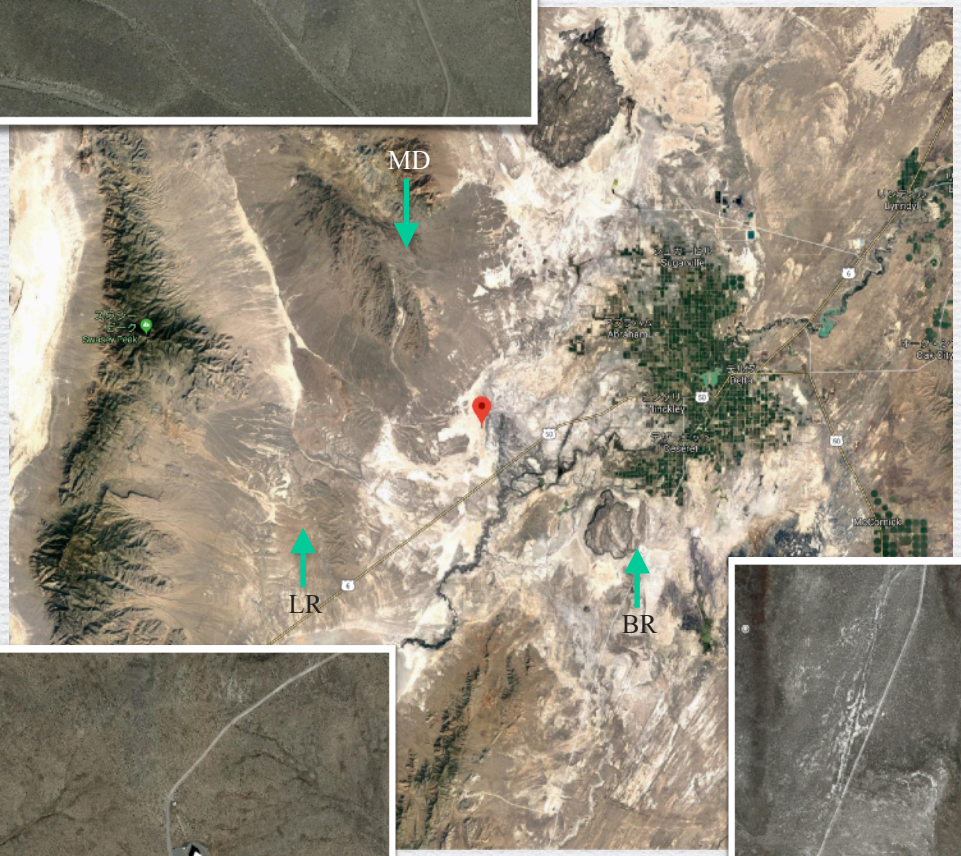

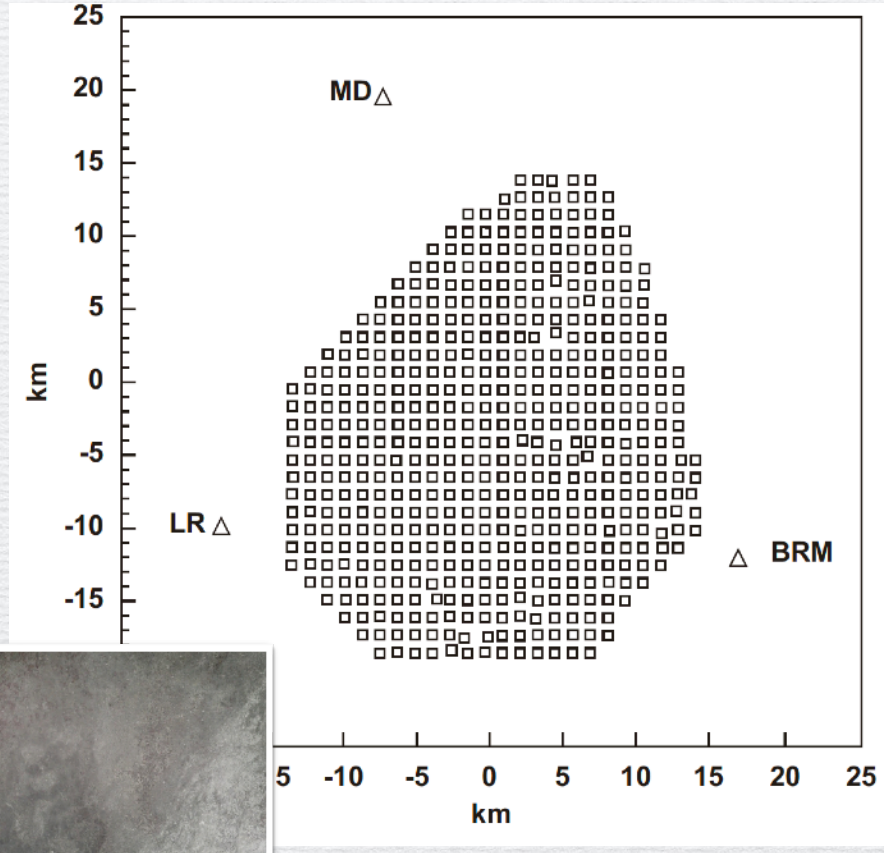

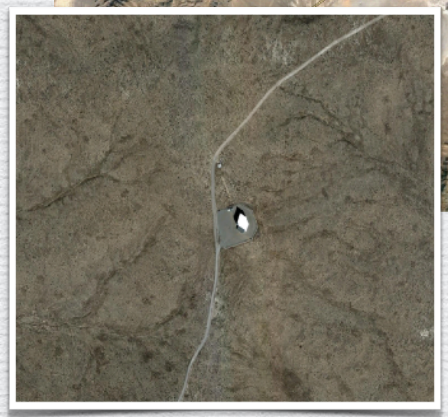

cated in the desert about 1400 m above sea level
and 112.9°W in Millard County, Utah, USA, about
of Salt Lake City. A control center to support

Telescope Array
FD

[tok11, abu12,]

12 fluorescence detector telescopes at 3 sites

Primary mirror (3.3mϕ) and (16×16) PMT camera

18° azimuthal 15° elevation field of view / telescope

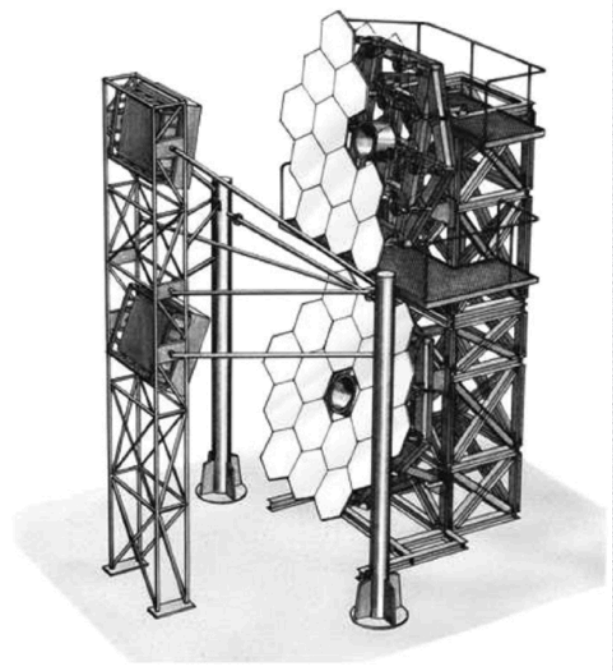

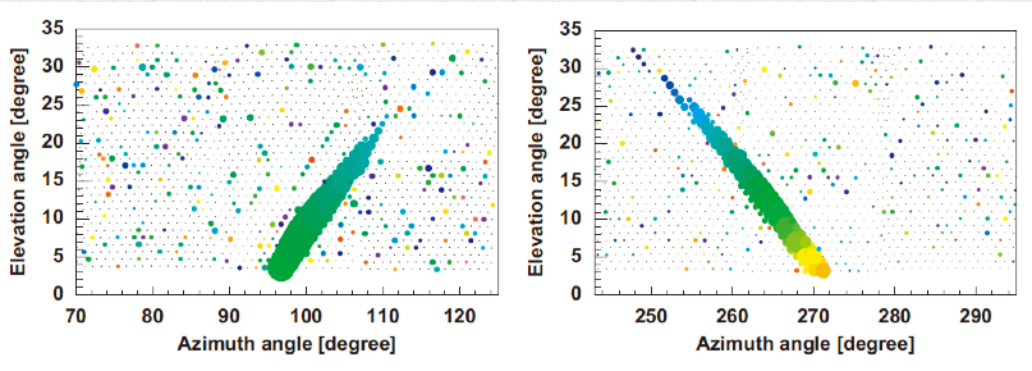

Telescope Array
SD

[tok11, abu12,]

700 km² (~30kmϕ)

507 plastic scintillation counter of 3m²×1.2cm×2 layers

mean distance 1.2 km on square grid

~0.7 SD / km²

104 wavelength-shifting fibers
PMT 9124SA; Electron Tubes Ltd.
12bit 50 MHz FADC
Time recording calibrated by GPS.

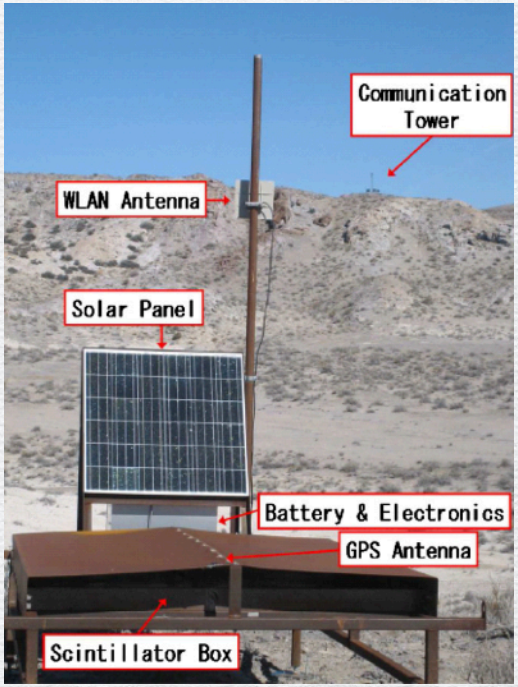

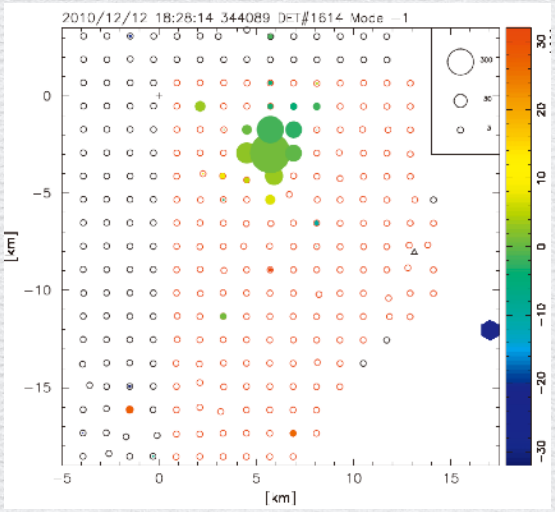

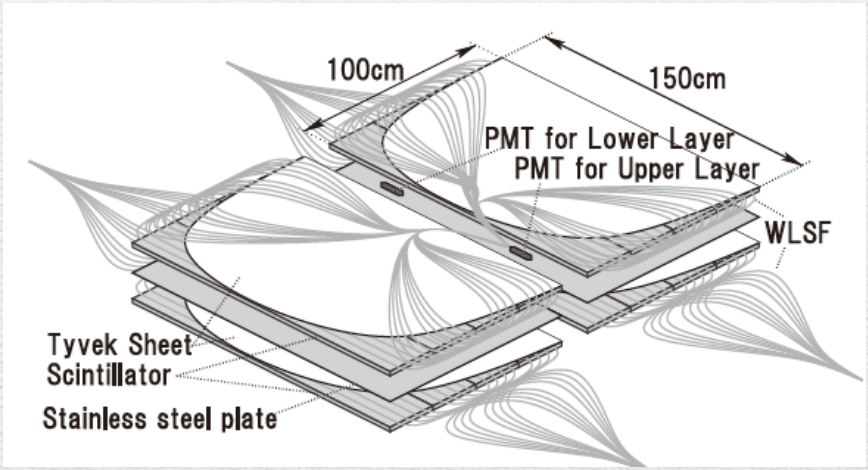

Analysis Methods

Analysis Methods
Event Reconstruction

[aug15]

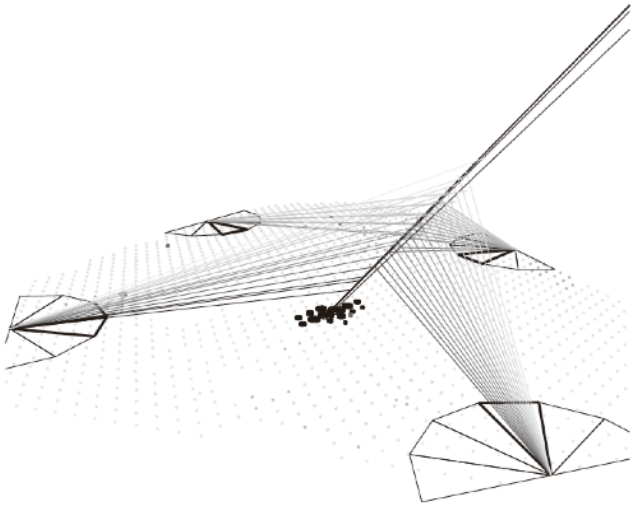

Fig. 33. Geometry reconstruction of an event observed by four telescopes and the surface detector.

Direction of CR: time difference of SD signals

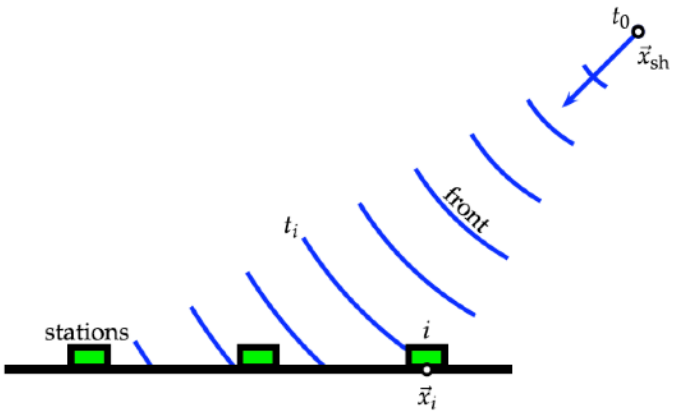

Fig. 35. Reconstruction of shower geometry: schematic representation of the evolution of the shower front.

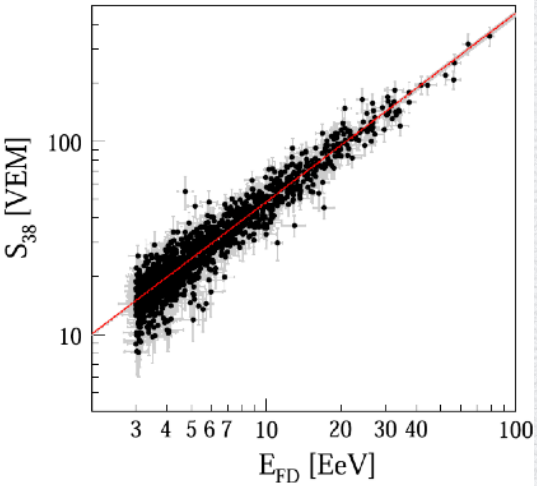

Fig. 41. Correlation between S_{38} and E_{FD} [11,122].

Absolute energy: sum of the FD signal
with correction
atmospheric attenuation
escaped events (muon, neutrino) ~10%
systematic uncertainty: 14%

The signal size (θ=38°) of SD:
correlated with CR energy, calibrated to FD.

VEM: Vertical Equivalent Muon

Ultra-High-Energy Cosmic Rays (UHECRs)

[anc19]

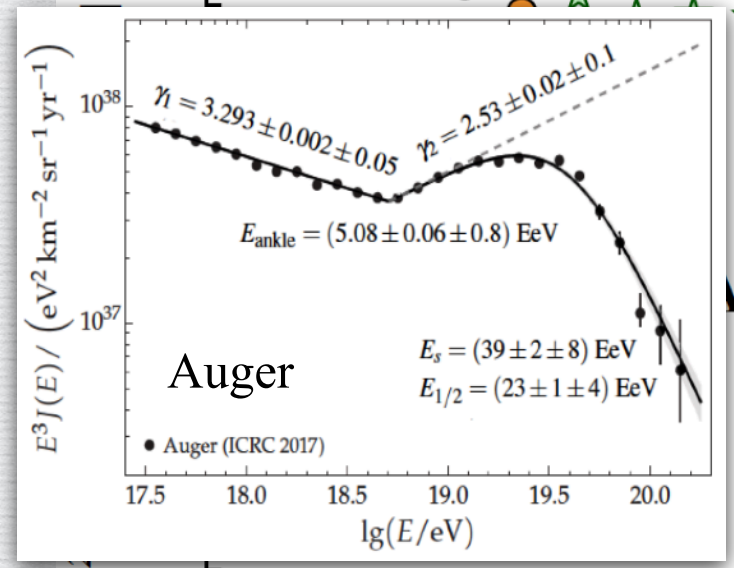

Analysis Methods
FD

[anc19]

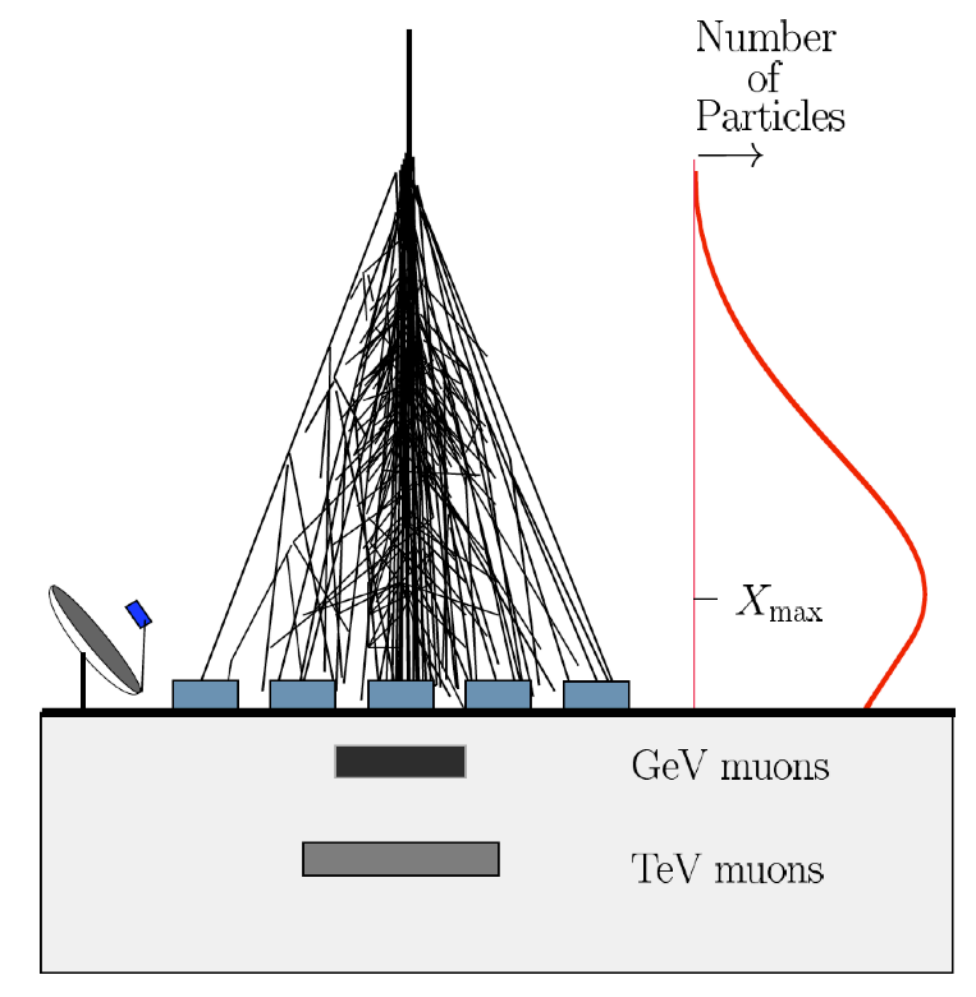

X_{max}:
atmospheric depth by FD data where the maximum number of particles is the largest.

$\langle X_{max} \rangle$: mean of X_{max}

$\sigma(\langle X_{max} \rangle)$: standard deviation of X_{max}

for the events of interest

$\langle X_{max} \rangle$ and $\sigma(\langle X_{max} \rangle)$ are predicted to be correlated with the mass (A) of the primary CR.

The correlation depends on the hadronic shower model.

Primary beam energy is above where accelerate laboratory data are available.

X_{max} distribution predictions

[aab14]

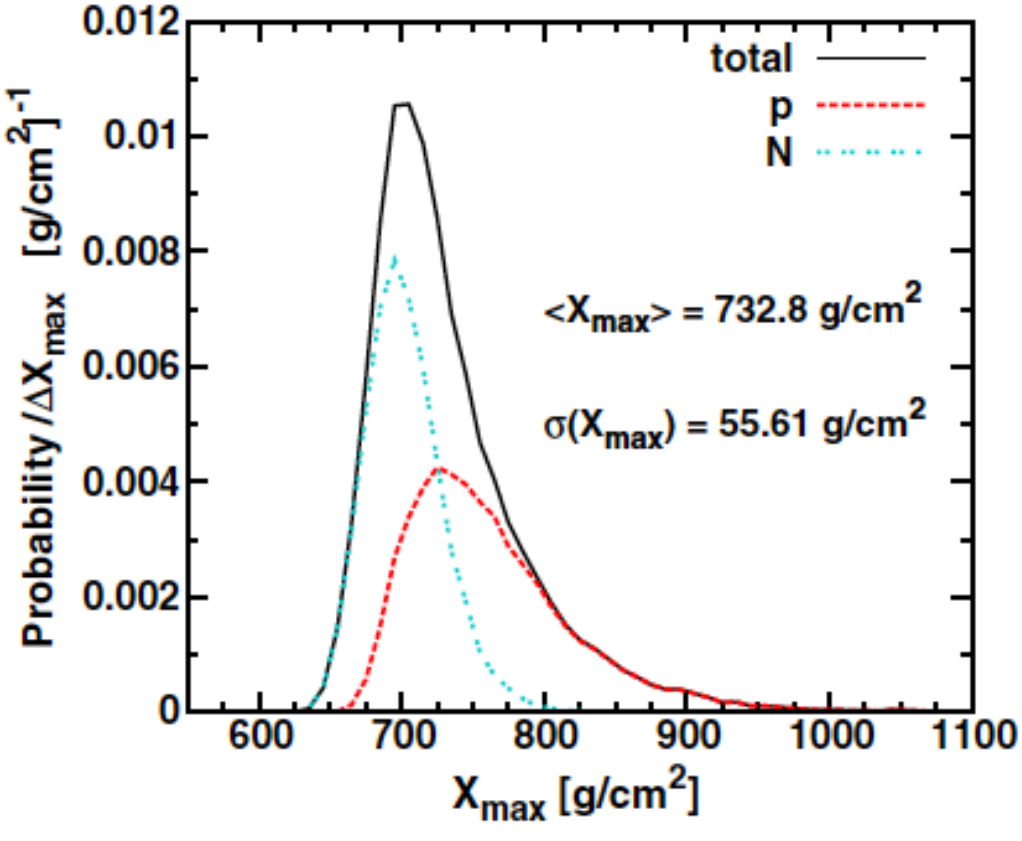

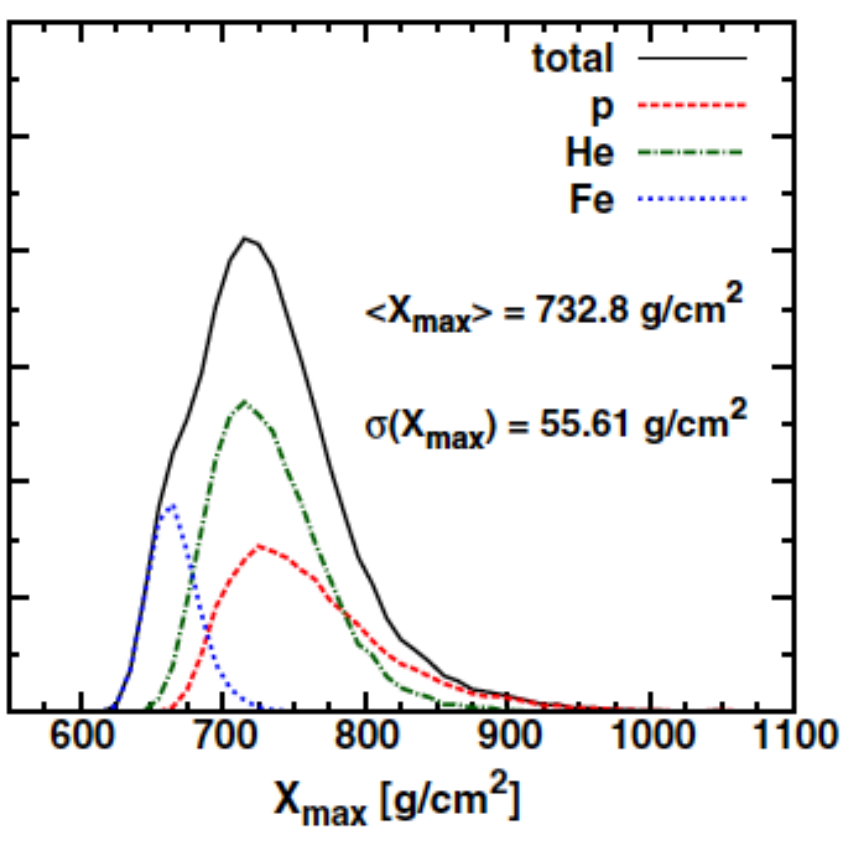

Composition

Mass Composition

[aab14]

Pierre Auger Observatory

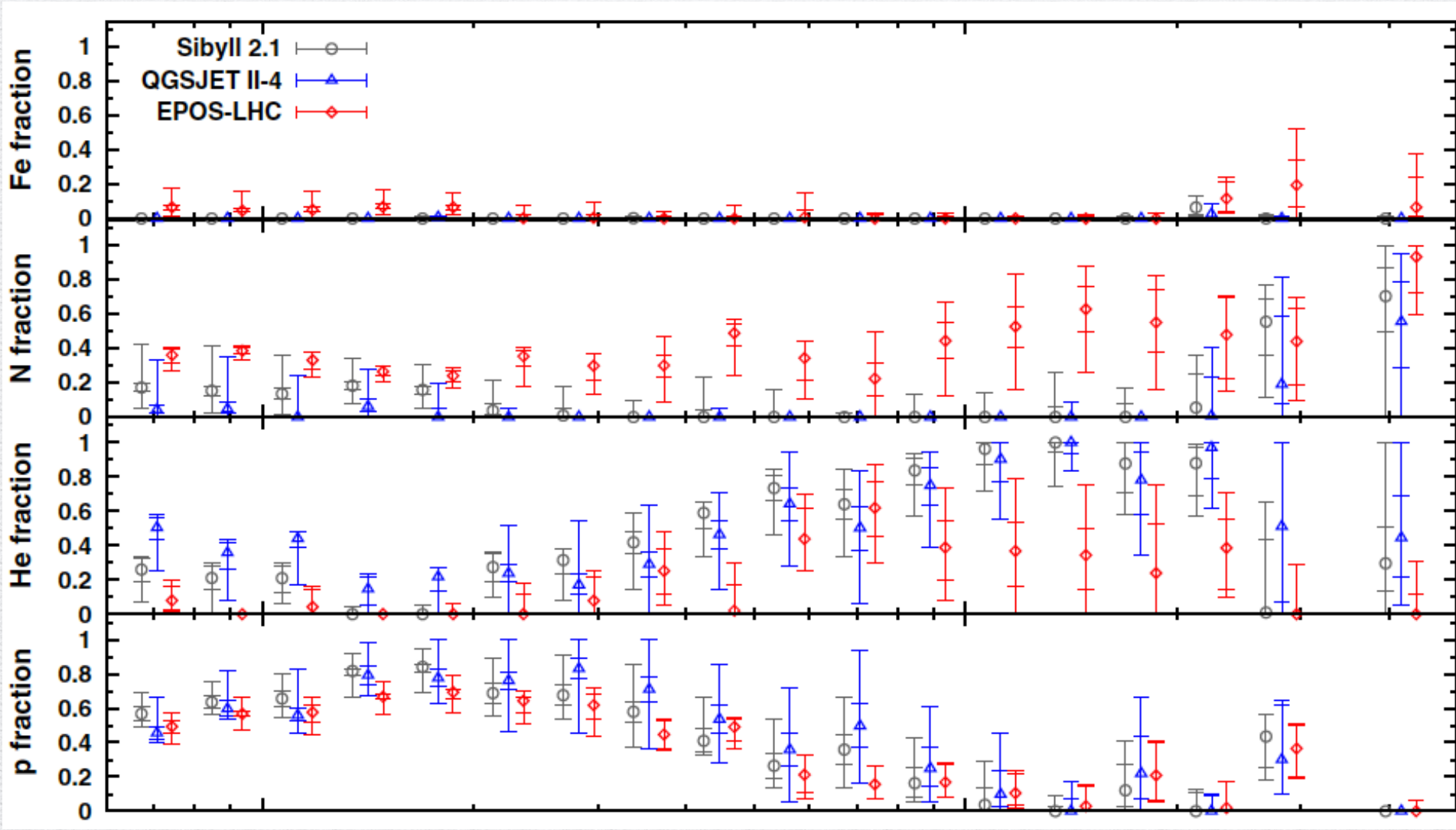

Mass Composition

[gor18]

Pierre Auger Observatory

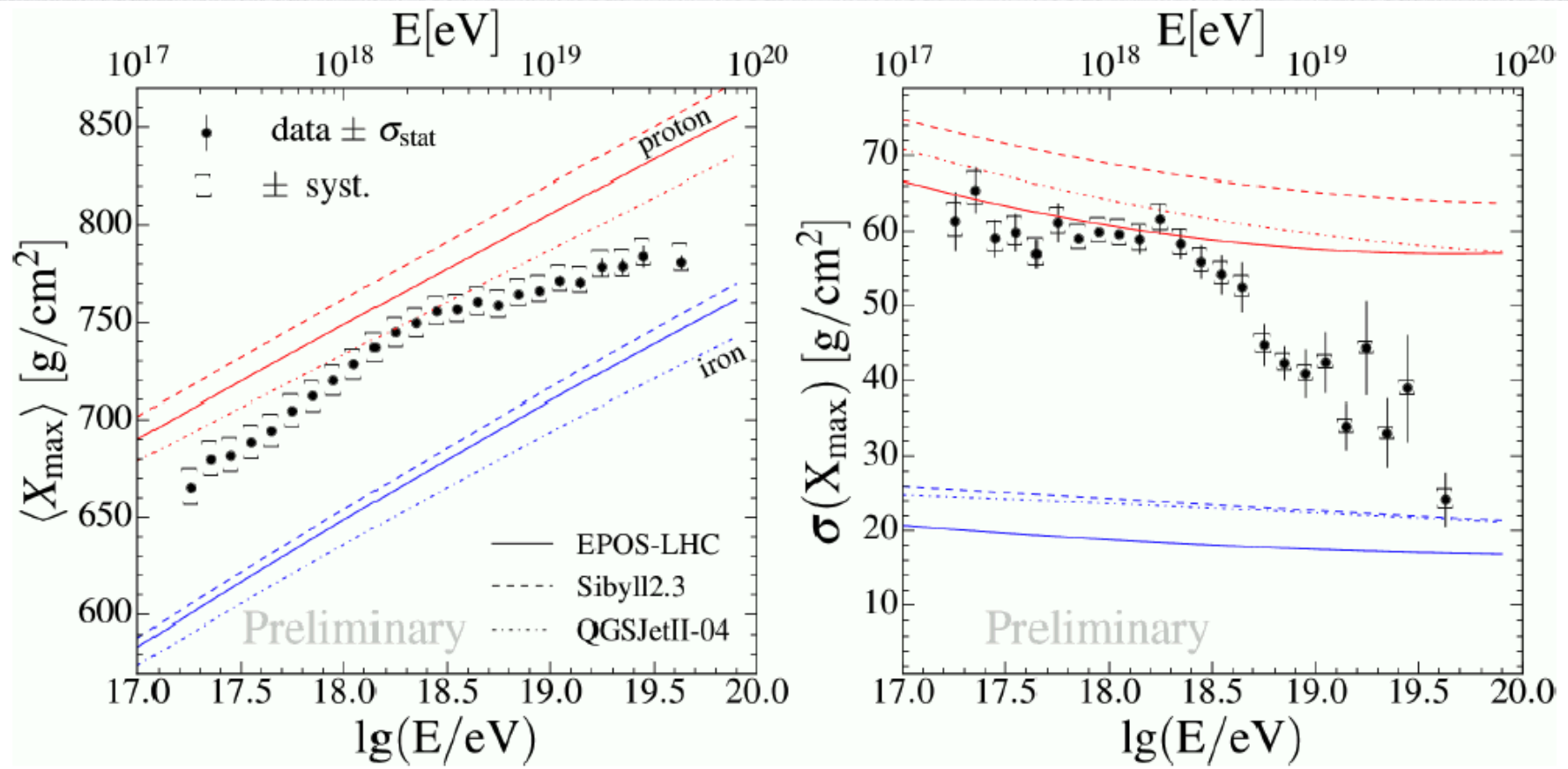

The fraction of proton increases up to $10^{18.3}$ eV and then decreases.

Composition of heavier mass nuclei are becoming dominating at the highest energy.

Mass Composition

[abb19]

Telescope Array

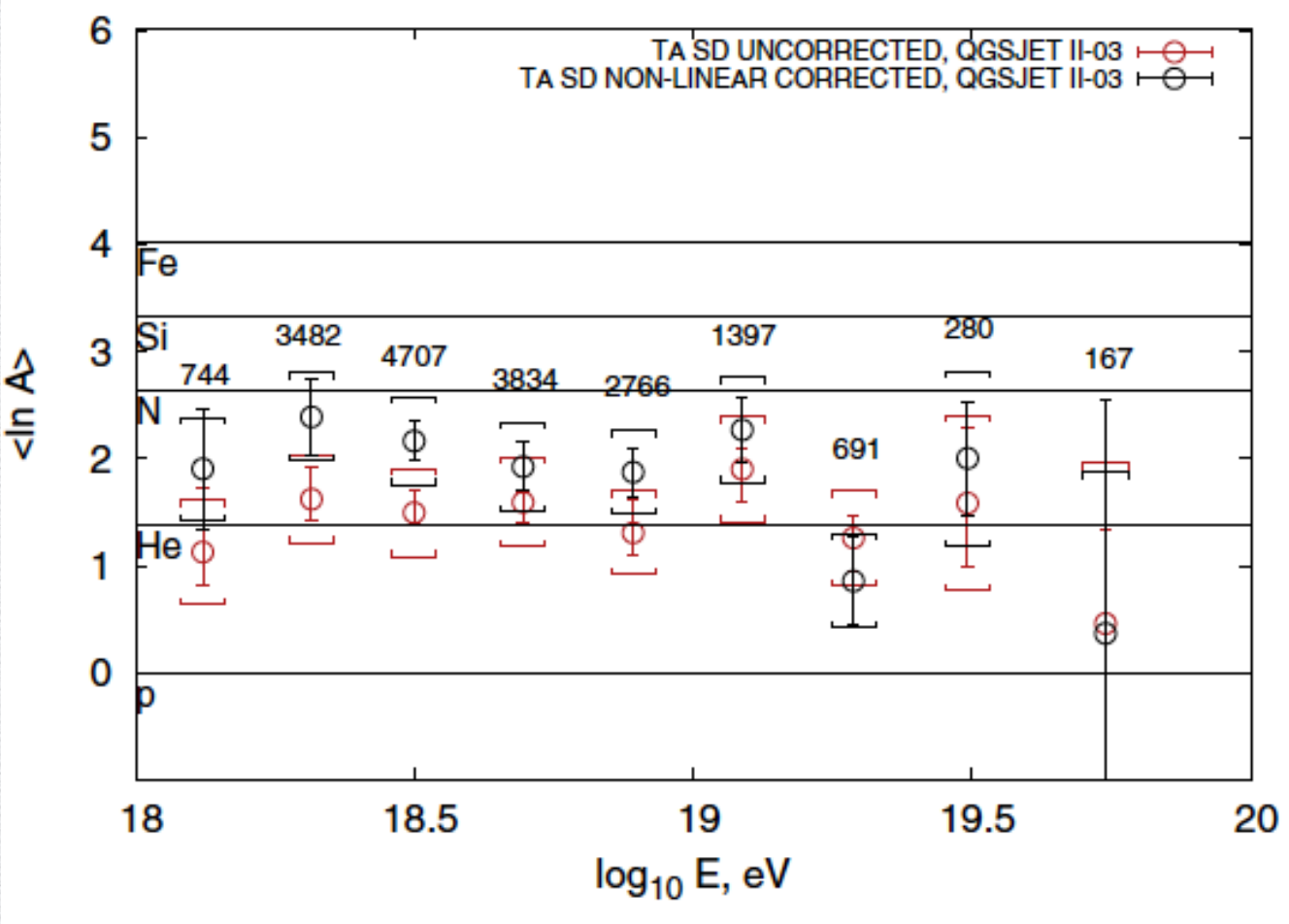

TA data also show heavier nuclei at high-energy with flatter energy dependence than Auger.

Mass Composition

[mol18]

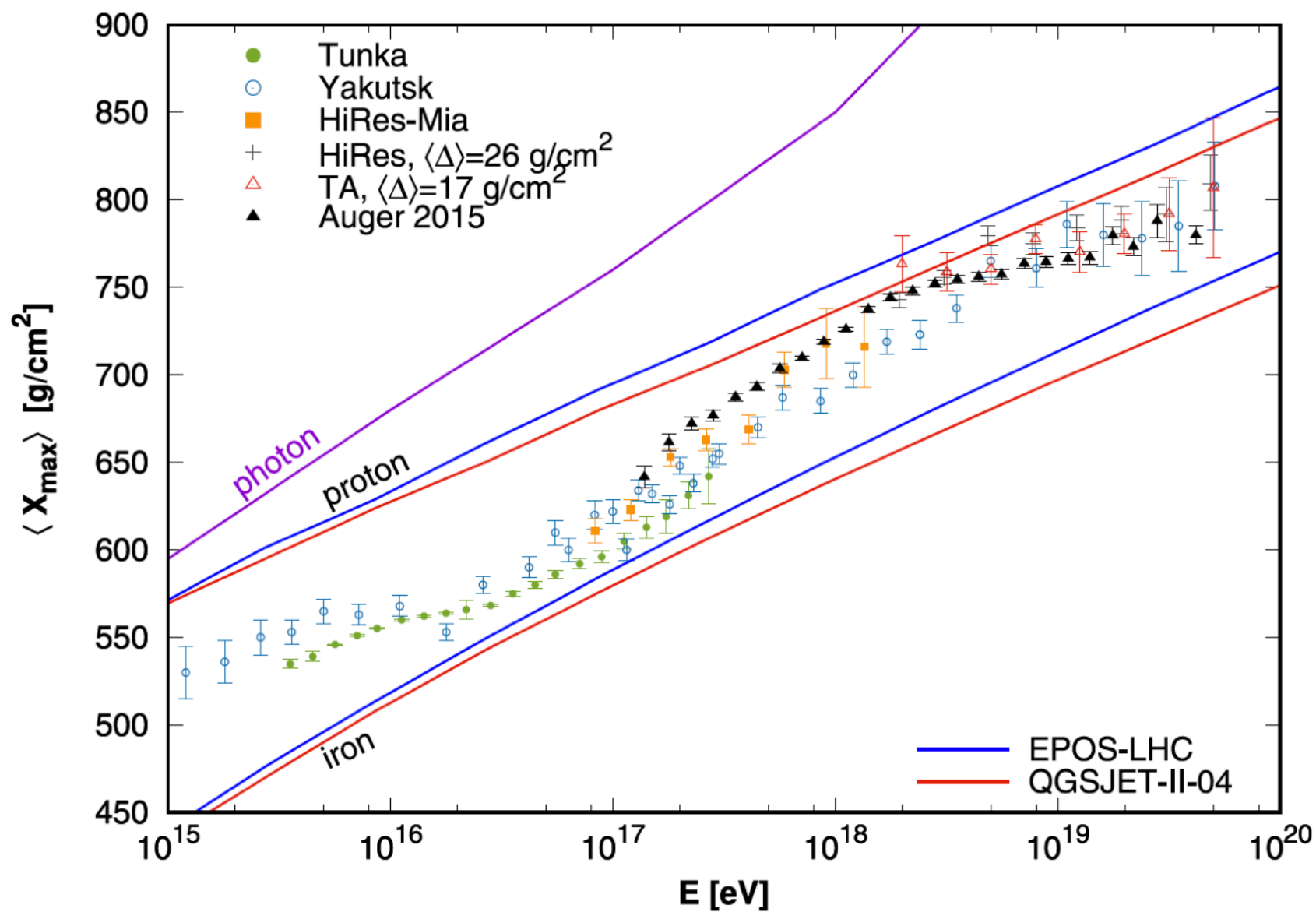

Energy Loss Process in Space Propagation

Greisen, Zatzepin, and Kuzmin (GZK) Cutoff [gre66,zat66]

GZK predicted a cutoff of UHECR flux at around 10^{20} eV
due to energy-loss with the collision of CMB in extragalactic propagation

For UHECR protons

pion-production by scattering with CMB

p+photon → $\pi^{\pm}$ production

For UHECR nuclei

photo-absorption of CMB

→ excitation to GDR

→ disintegration (photo-disintegration)

Cosmic Microwave Background (CMB)

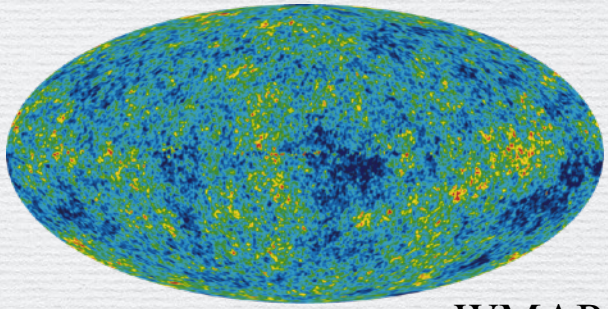

WMAP

T=2.72548±0.00057 K

Energy-loss process of UHECR is a key point to understood the energy distribution and composition of UHECRs and their origin, production mechanism, and the propagation.

Energy Loss Process of UHECRs in Extragalactic Propagation

[all12, kha05]

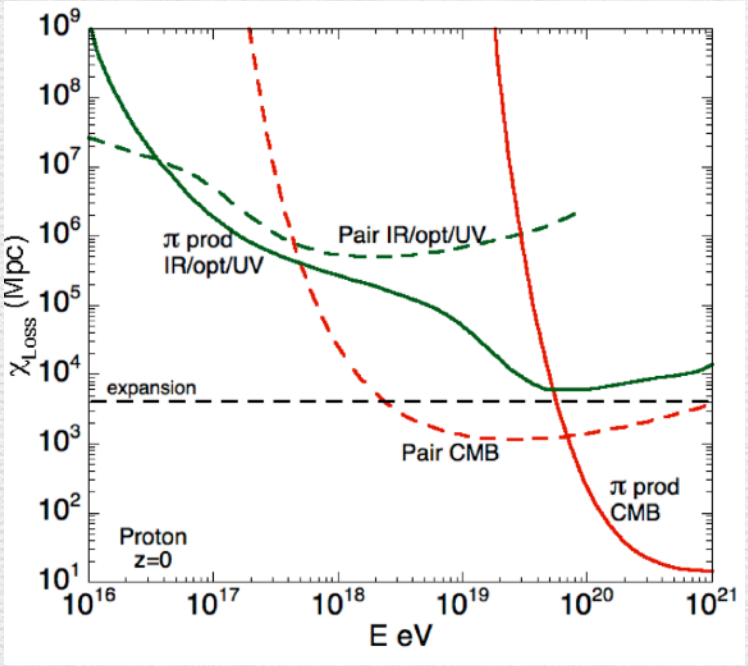

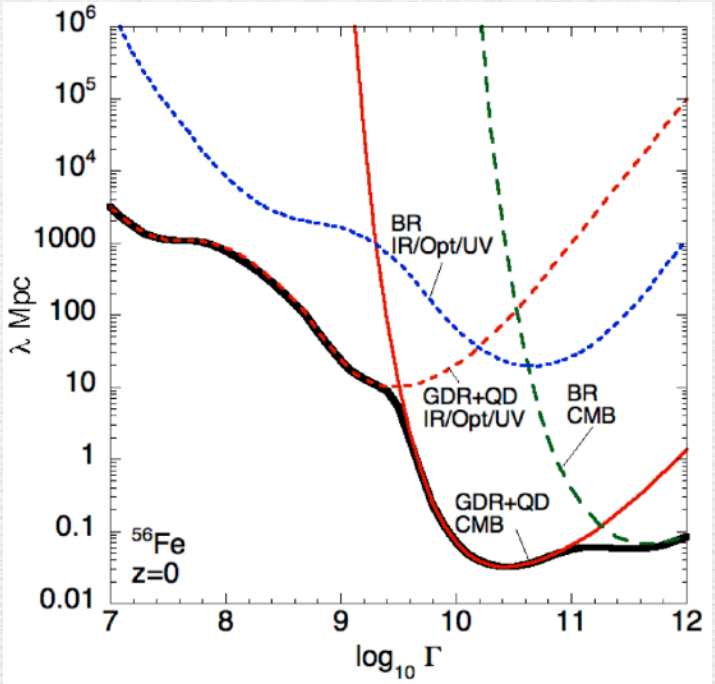

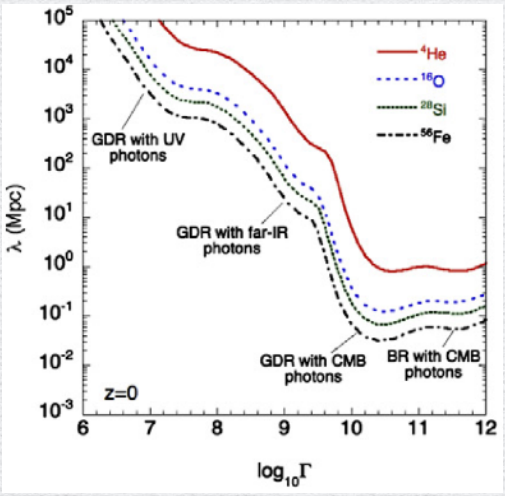

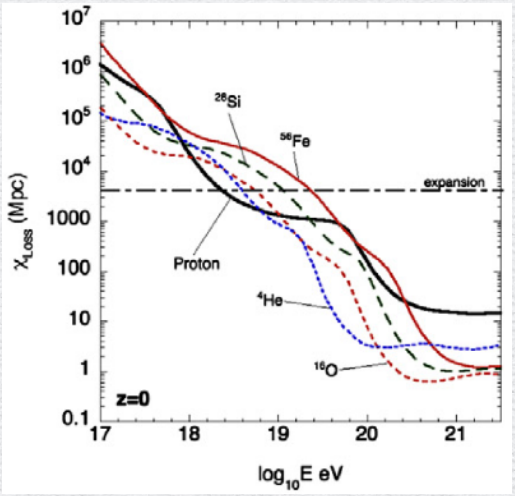

Refinements of the theoretical model in [kha05]

[ste99]

Unfortunately, photodisintegration cross section data are incomplete. For many reaction channels, $\sigma(\epsilon)$ data do not exist. Also, integrated cross section strengths are not available for all of the exclusive channels. The most complete compilation of the world's GDR cross section data exists in the 15 volumes of Fuller & Gerstenberg (1983). In these volumes GDR cross section data for ^{56}Fe, for example, are given only for the (γ, pX) channel and the inverse channels (α, γ) and (p, γ).

Energy Loss Process of UHECRs in Extragalactic Propagation

[anc19]

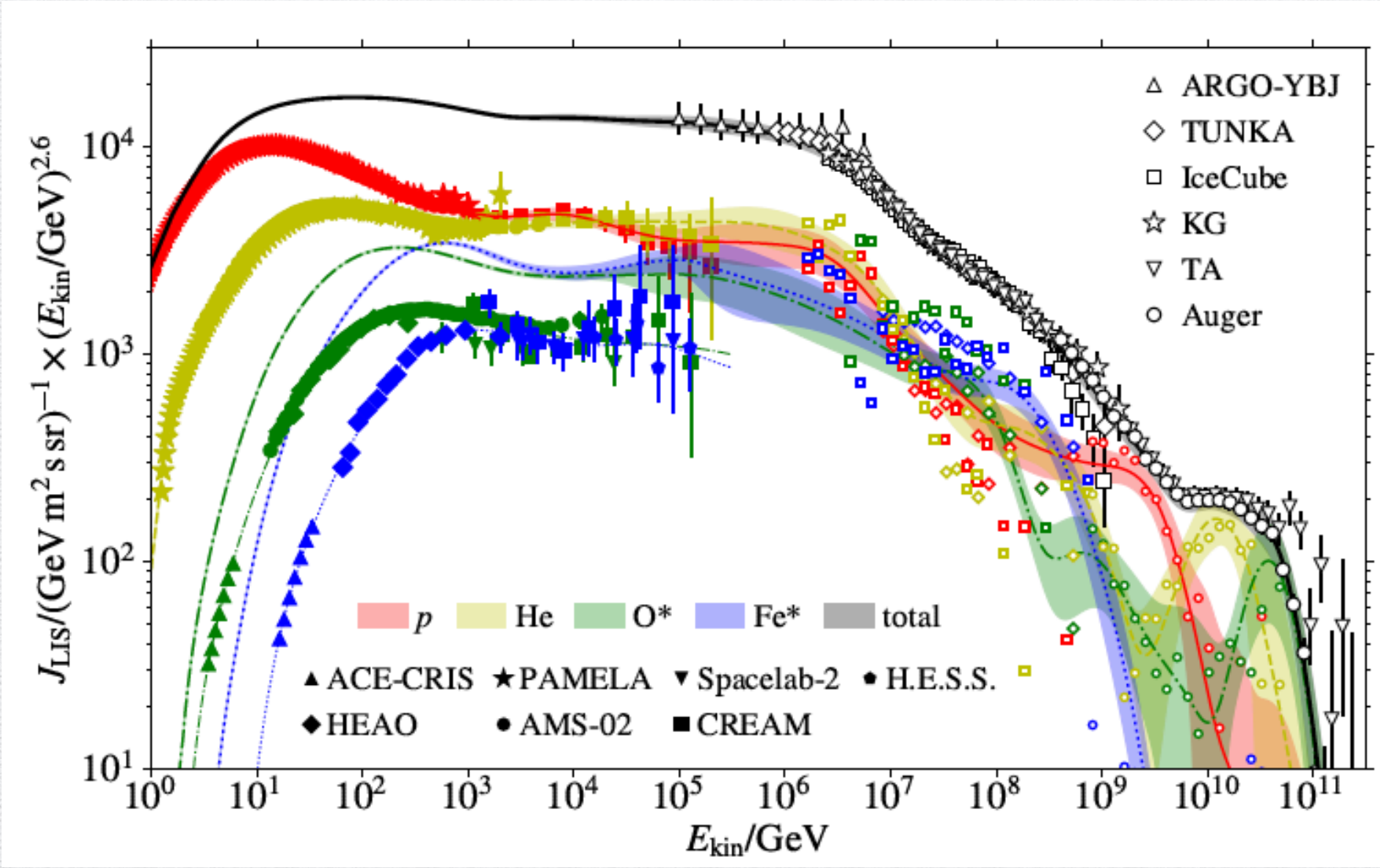

PANDORA Project

PANDORA Project:

Photo-**A**bsorption of **N**uclei and **D**ecay **O**bservation for **R**eaction in **A**strophysics

Systematic Measurement on E1 Strength Distribution and n,p,α,γ decays up to A~56

as a joint project of the three facilities

RCNP-Grand Raiden

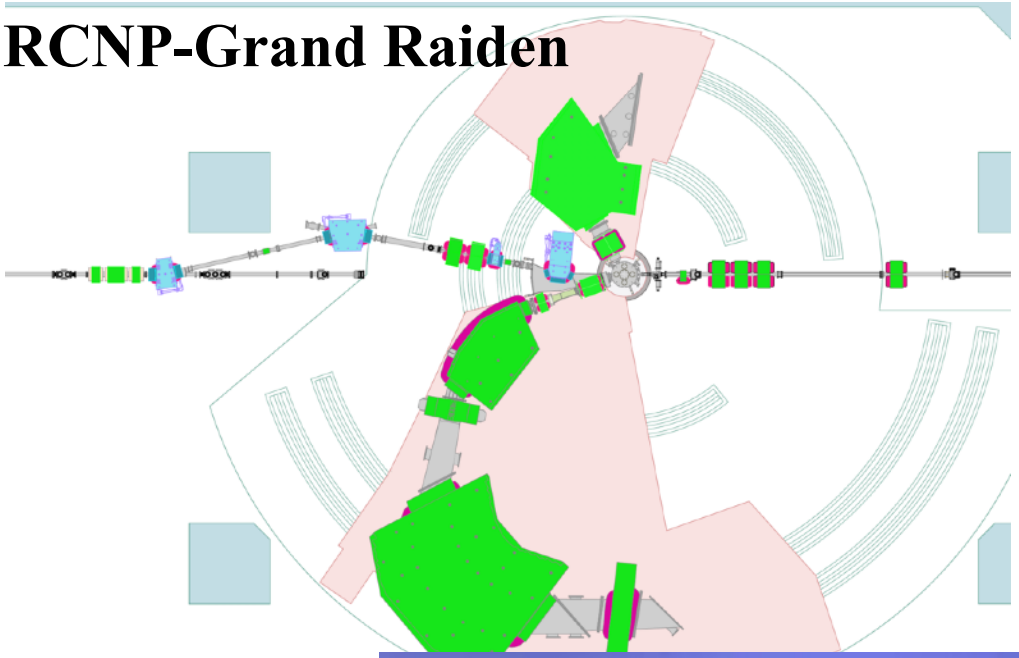

iThembaLABS

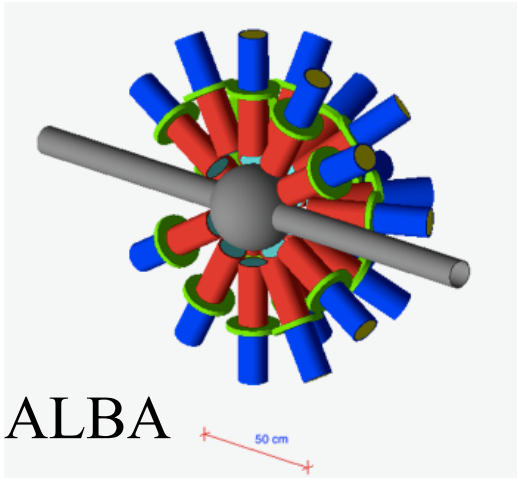

ELI-NP

Combination of experiments with complementary devices.

CAKE

decay charge particle detector array

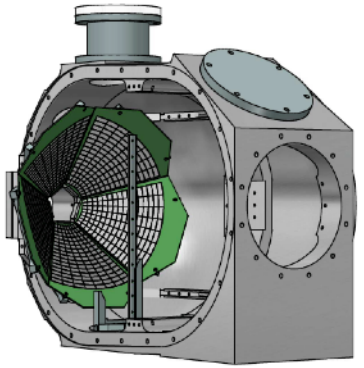

Systematic Measurement on E1 Strength Distribution and n,p,α,γ decays up to A~56

- E1 excitation strength distribution
- n, p, α, γ decay branching ratios
- from light to A~56 for stable nuclei

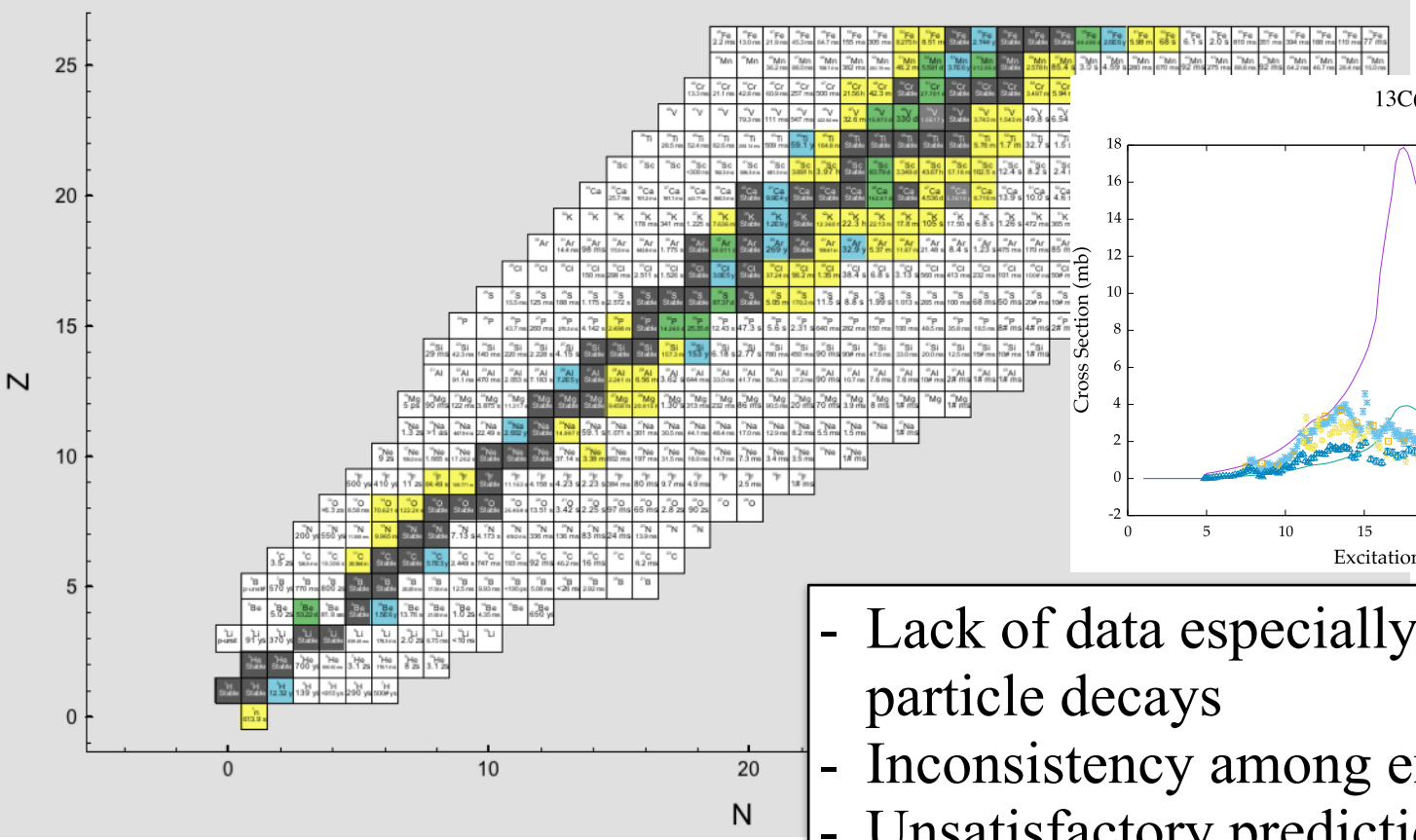

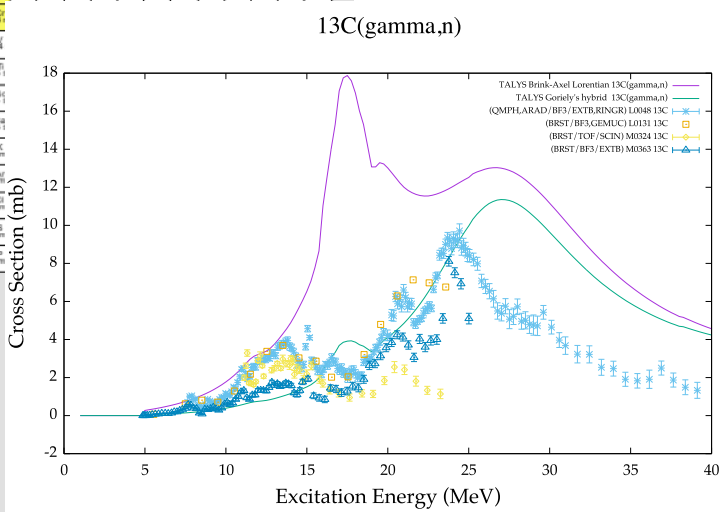

- Lack of data especially for charged particle decays
- Inconsistency among experiments
- Unsatisfactory prediction by models

Photo-disintegration Pass of ^{56}Fe

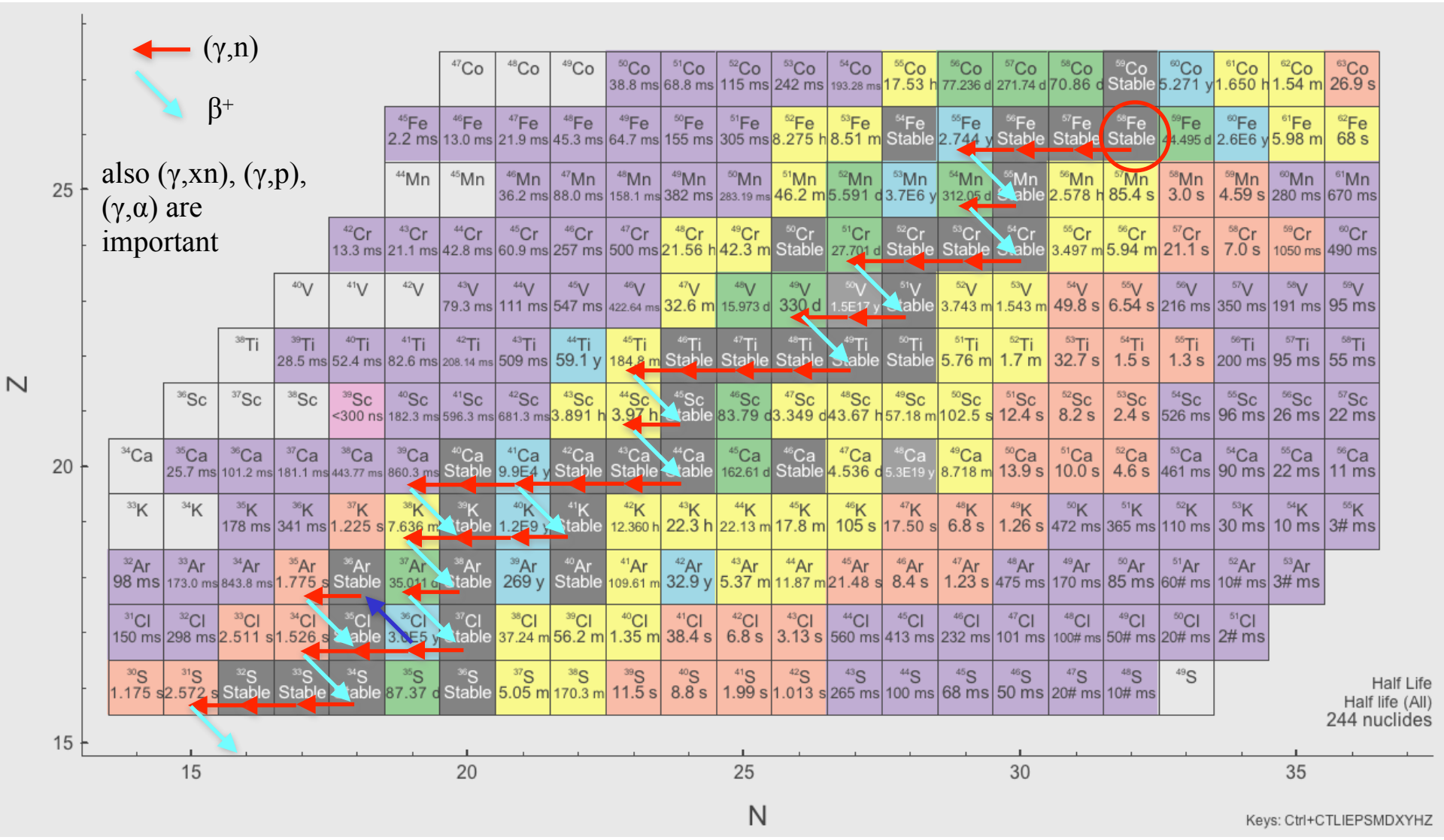

Photo-disintegration Pass of ^{56}Fe

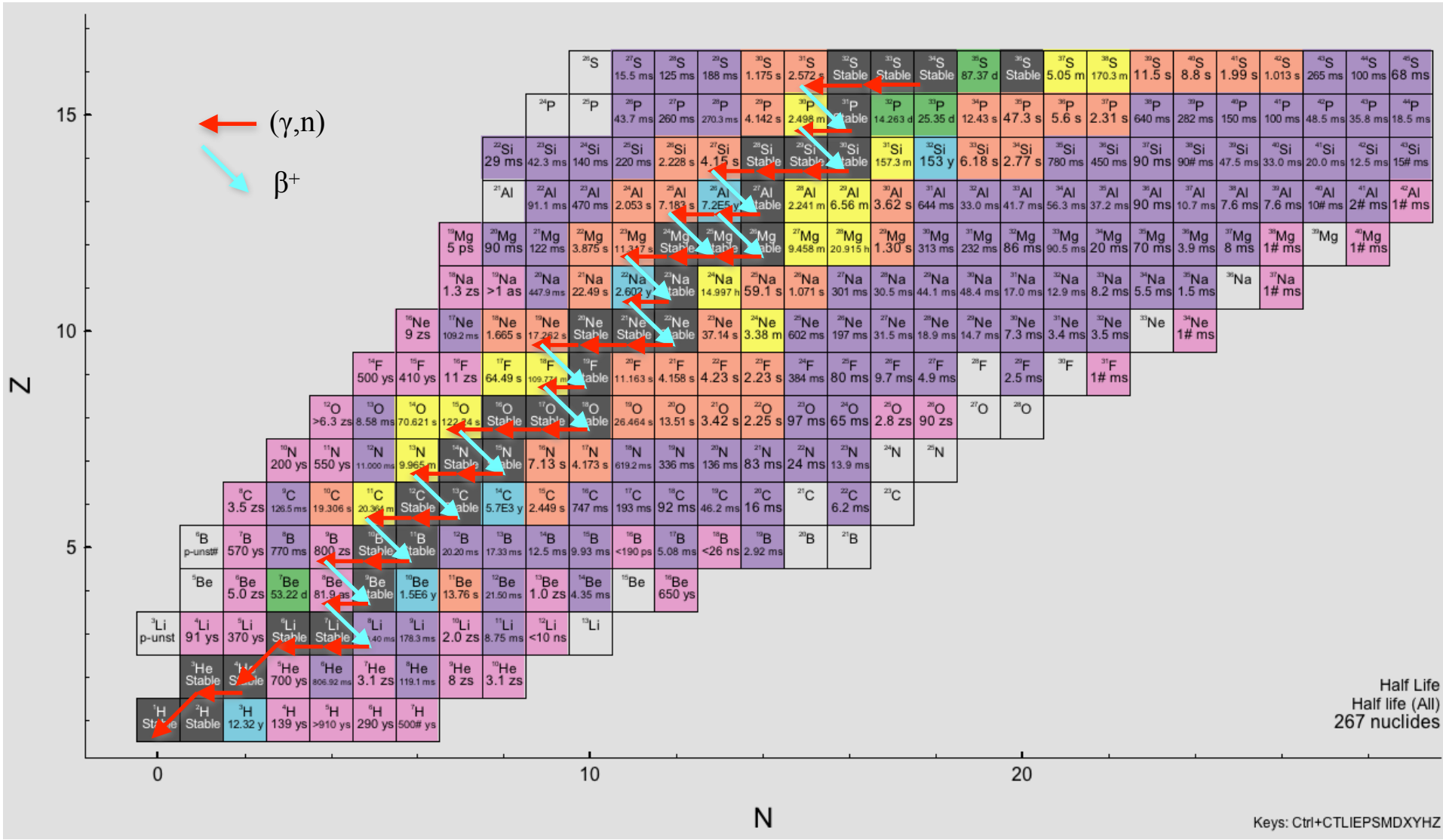

Photo-disintegration Pass of ^{56}Fe

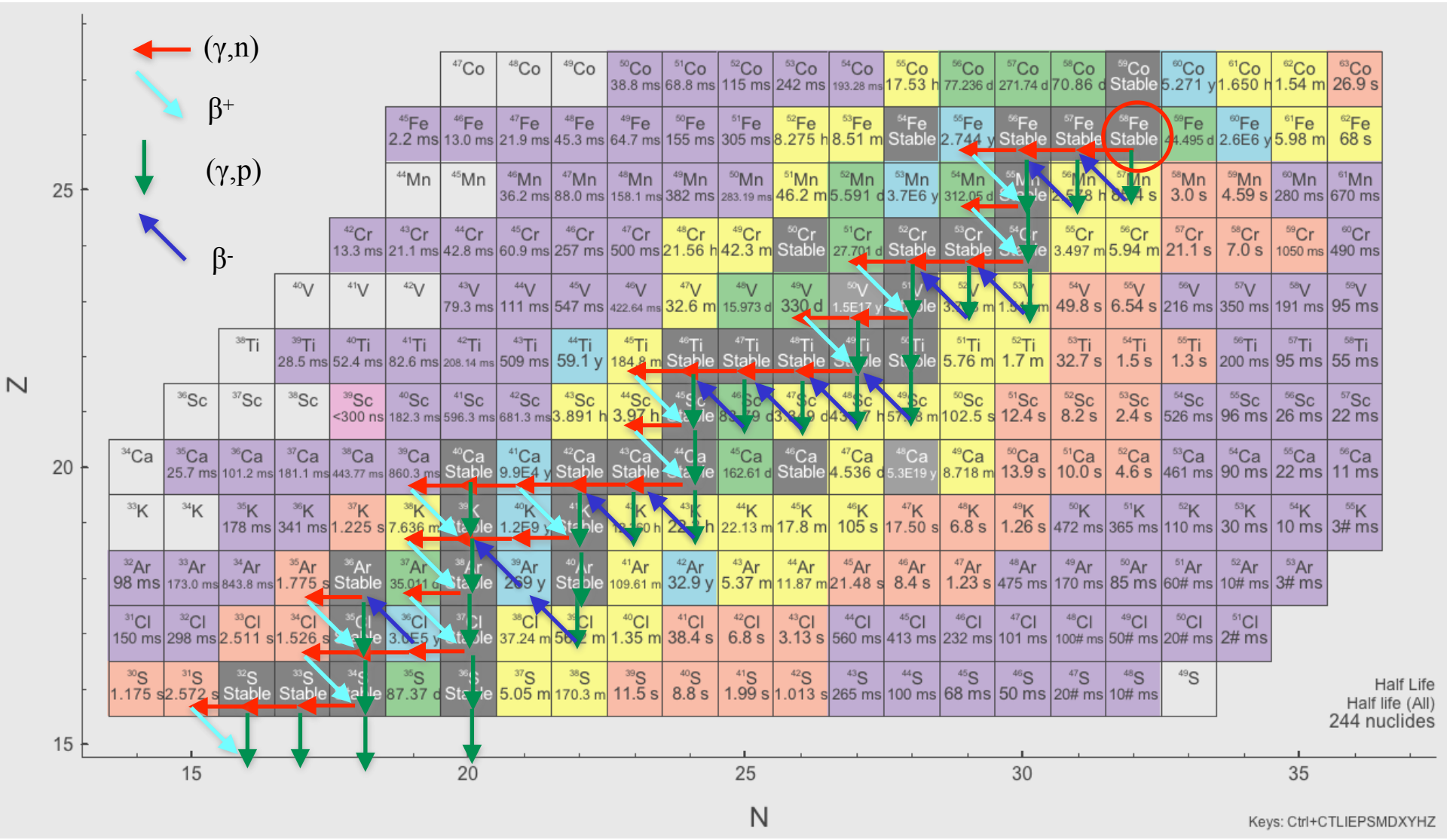

Also (γ,xn), (γ,α) are important

Unstable nuclei are also relevant up to $T_{1/2}$~1 min

Systematic Measurement on E1 Strength Distribution and n,p,α,γ decays up to A~56

- E1 excitation strength distribution
- n, p, α, γ decay branching ratios
- from light to A~56 for stable nuclei

Motivations

- High-quality systematic data for nuclear structure models, nuclear astrophysics, and applications
- Photo-disintegration process of ultra-high-energy cosmic rays by absorbing CMB photons in extragalactic propagation

Systematic Measurement on E1 Strength Distribution and n,p,α,γ decays up to A~56

RCNP (proton Coulomb excitation) AT, N. Kobayashi, T. Shima, T. Sudo et al.,

- E1 excitation up to 32 MeV
- γ-decay

iThemba LABS (proton Coulomb excitation) L. Pellegri, R. Neveling, F.D. Smit et al.,

- E1 excitation up to 24 MeV
- p,α,γ-decays

ELI-NP (gamma-beam excitation) D. Balabanski, P-A Söderström, L. Capponi et al.,

- good calibration of the absolute c.s.
- n, p,α,γ-decays up to 20 MeV

Keeping good consistency among the three facilities and different beam times using a reference target (^{27}Al).

Theoretical supports

D. Allard, B. Baret, E. Khan, J. Kiener, S. Nagataki, E. Parizot, T. Vincent et al.,

Anisotropy

Anisotropy

[aab15,aug17]

Pierre Auger Observatory

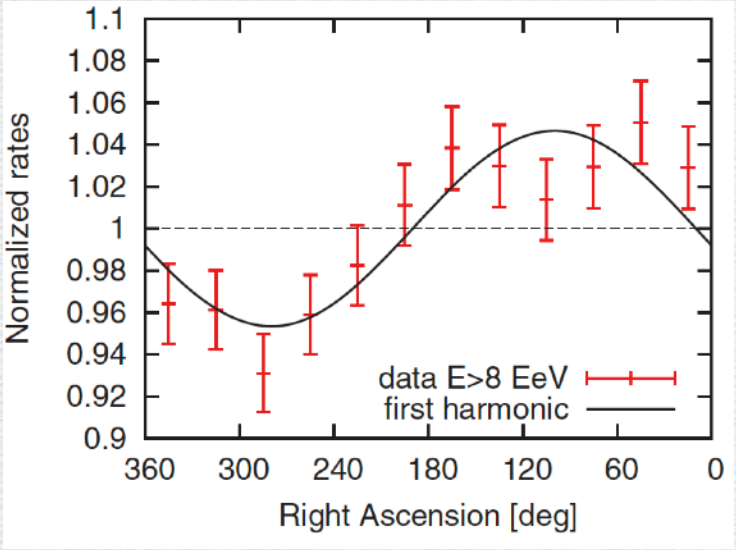

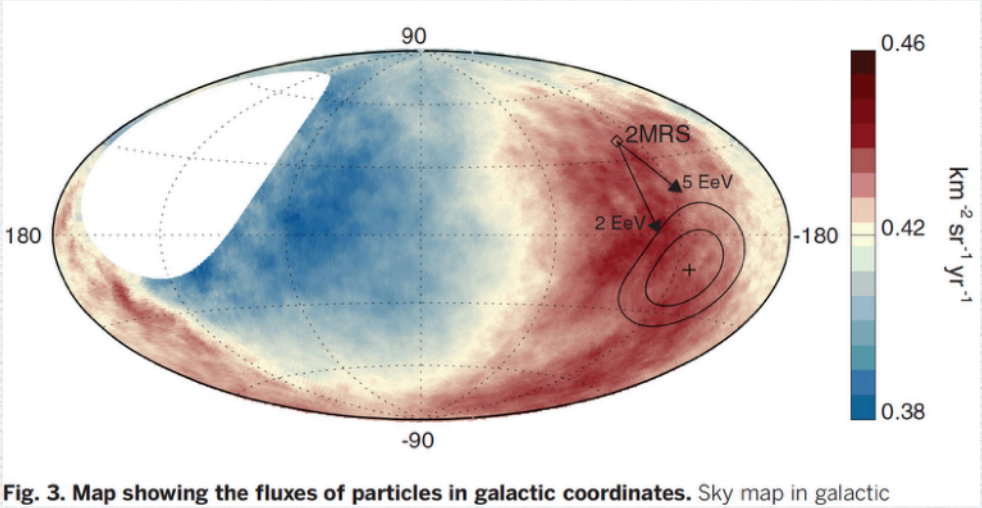

Fig. 3. Map showing the fluxes of particles in galactic coordinates. Sky map in galactic

Anisotropy by dipole fit (5.2σ)

Anisotropy after subtracting the isotropic component is analyzed.

Anisotropy is an important indicator of the sources of UHECRs and their distribution.

Anisotropy

Pierre Auger Observatory

[aab18]

Table 1
Populations Investigated

SBGs	l (°)	b (°)	Distance[a] (Mpc)	Flux Weight (%)	Attenuated Weight: A/B/C (%)	% Contribution[b]: A/B/C (%)
NGC 253	97.4	−88	2.7	13.6	20.7/18.0/16.6	35.9/32.2/30.2
M82	141.4	40.6	3.6	18.6	24.0/22.3/21.4	0.2/0.1/0.1
NGC 4945	305.3	13.3	4	16	19.2/18.3/17.9	39.0/38.4/38.3
M83	314.6	32	4	6.3	7.6/7.2/7.1	13.1/12.9/12.9
IC 342	138.2	10.6	4	5.5	6.6/6.3/6.1	0.1/0.0/0.0
NGC 6946	95.7	11.7	5.9	3.4	3.2/3.3/3.5	0.1/0.1/0.1
NGC 2903	208.7	44.5	6.6	1.1	0.9/1.0/1.1	0.6/0.7/0.7
NGC 5055	106	74.3	7.8	0.9	0.7/0.8/0.9	0.2/0.2/0.2
NGC 3628	240.9	64.8	8.1	1.3	1.0/1.1/1.2	0.8/0.9/1.1
NGC 3627	242	64.4	8.1	1.1	0.8/0.9/1.1	0.7/0.8/0.9
NGC 4631	142.8	84.2	8.7	2.9	2.1/2.4/2.7	0.8/0.9/1.1
M51	104.9	68.6	10.3	3.6	2.3/2.8/3.3	0.3/0.4/0.5
NGC 891	140.4	−17.4	11	1.7	1.1/1.3/1.5	0.2/0.3/0.3
NGC 3556	148.3	56.3	11.4	0.7	0.4/0.6/0.6	0.0/0.0/0.0
NGC 660	141.6	−47.4	15	0.9	0.5/0.6/0.8	0.4/0.5/0.6
NGC 2146	135.7	24.9	16.3	2.6	1.3/1.7/2.0	0.0/0.0/0.0
NGC 3079	157.8	48.4	17.4	2.1	1.0/1.4/1.5	0.1/0.1/0.1
NGC 1068	172.1	−51.9	17.9	12.1	5.6/7.9/9.0	6.4/9.4/10.9
NGC 1365	238	−54.6	22.3	1.3	0.5/0.8/0.8	0.9/1.5/1.6
Arp 299	141.9	55.4	46	1.6	0.4/0.7/0.6	0.0/0.0/0.0
Arp 220	36.6	53	80	0.8	0.1/0.3/0.2	0.0/0.2/0.1
NGC 6240	20.7	27.3	105	1	0.1/0.3/0.1	0.1/0.3/0.1
Mkn 231	121.6	60.2	183	0.8	0.0/0.1/0.0	0.0/0.0/0.0
γAGNs						
Cen A Core	309.6	19.4	3.7	0.8	60.5/14.6/40.4	86.8/56.3/71.5
M87	283.7	74.5	18.5	1	15.3/7.1/29.5	9.7/12.1/23.1
NGC 1275	150.6	−13.3	76	2.2	6.6/6.1/7.5	0.7/1.6/1.0
IC 310	150.2	−13.7	83	1	2.3/2.4/2.6	0.3/0.6/0.3
3C 264	235.8	73	95	0.5	0.8/1.0/0.8	0.4/1.3/0.5
TXS 0149 + 710	127.9	9	96	0.5	0.7/0.9/0.7	0.0/0.0/0.0
Mkn 421	179.8	65	136	54	11.4/48.3/14.7	1.8/19.1/2.8
PKS 0229-581	280.2	−54.6	140	0.5	0.1/0.5/0.1	0.2/2.0/0.3
Mkn 501	63.6	38.9	148	20.8	2.3/15.0/3.6	0.3/5.2/0.6
1ES 2344 + 514	112.9	−9.9	195	3.3	0.0/1.0/0.1	0.0/0.0/0.0
Mkn 180	131.9	45.6	199	1.9	0.0/0.5/0.0	0.0/0.0/0.0
1ES 1959 + 650	98	17.7	209	6.8	0.0/1.7/0.1	0.0/0.0/0.0
AP Librae	340.7	27.6	213	1.7	0.0/0.4/0.0	0.0/1.3/0.0
TXS 0210 + 515	135.8	−9	218	0.9	0.0/0.2/0.0	0.0/0.0/0.0
GB6 J0601 + 5315	160	14.6	232	0.4	0.0/0.1/0.0	0.0/0.0/0.0
PKS 0625-35	243.4	−20	245	1.3	0.0/0.1/0.0	0.0/0.5/0.0
I Zw 187	77.1	33.5	247	2.3	0.0/0.2/0.0	0.0/0.0/0.0

Studying the correlation between the UHECR anisotropy and the distribution of galaxies from the 2FHL catalog (FERMI-LAT)

SBG: star burst galaxy

γAGN: γ-active galactic nucleus

Anisotropy

[aab18]

Pierre Auger Observatory

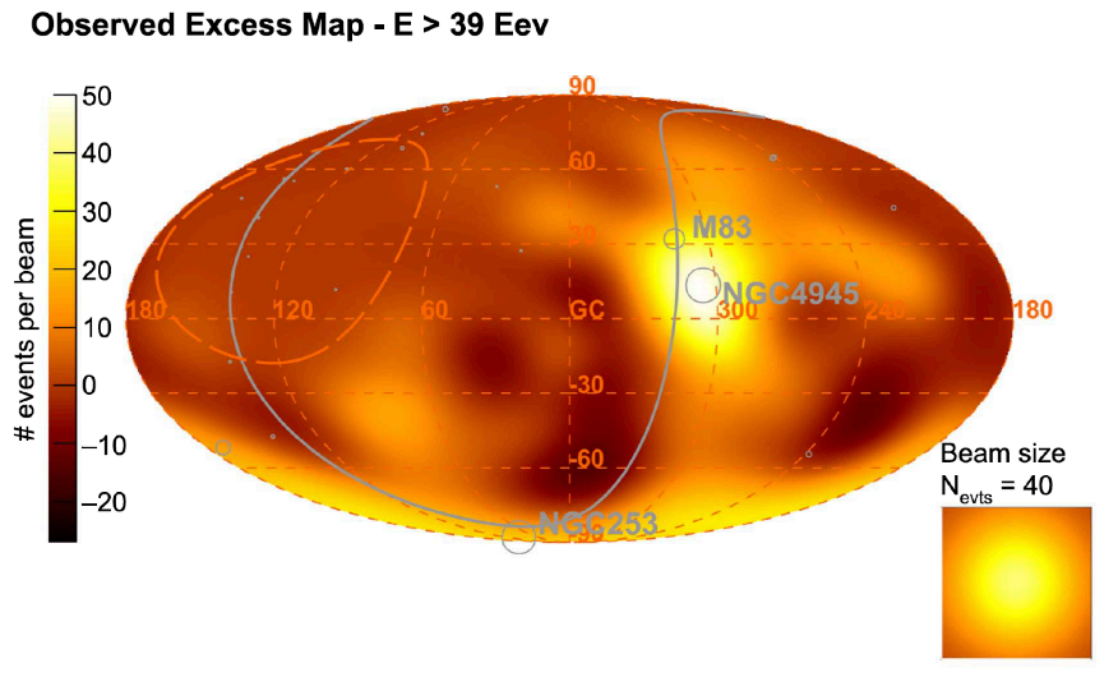

The observed anisotropy showed correlation with the distribution of SBGs (4.0σ).

SBG: star burst galaxy

γAGN: γ-active galactic nucleus

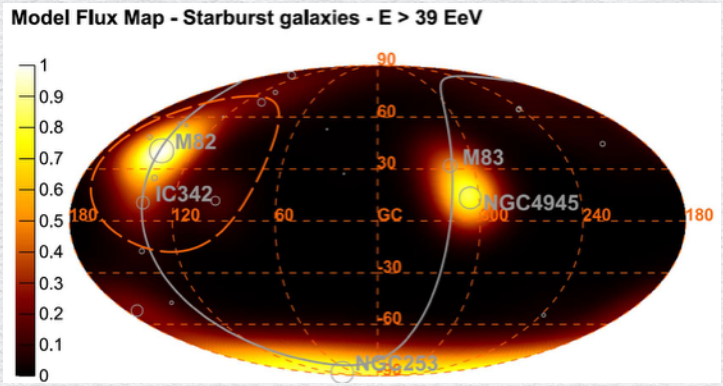

Prediction of UHECR intensity assuming SBGs as the source including attenuation in the extragalactic propagation.

Note that the region (surrounded by the dashed line) close to M82 is not covered by Auger.

Anisotropy

[aab18]

Pierre Auger Observatory

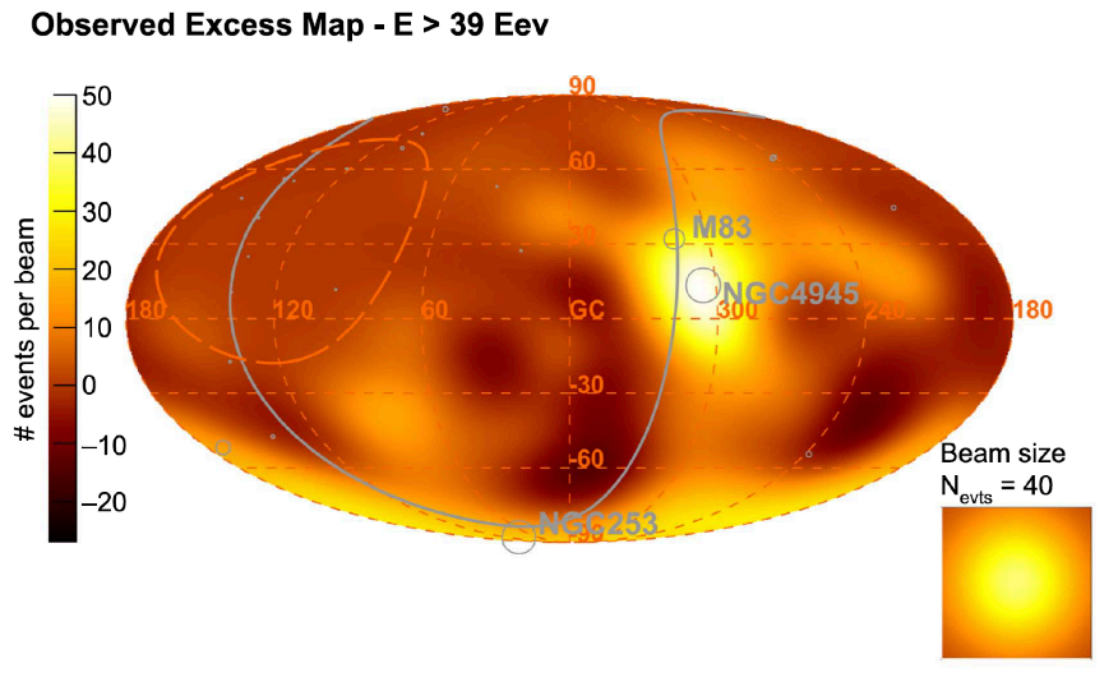

The observed anisotropy showed correlation with the distribution of SBGs (4.0σ).

SBG: star burst galaxy

γAGN: γ-active galactic nucleus

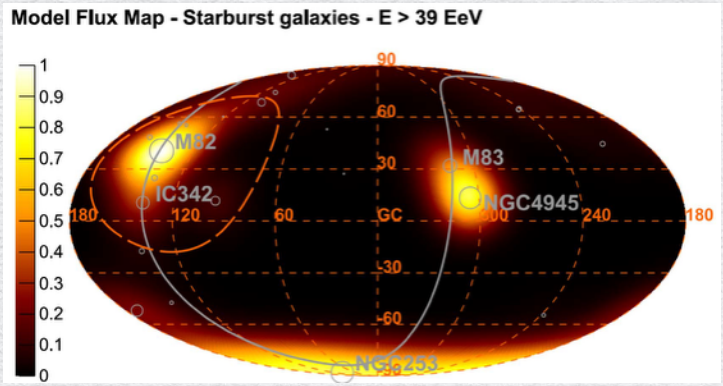

Prediction of UHECR intensity assuming SBGs as the source including attenuation in the extragalactic propagation.

Note that the region (surrounded by the dashed line) close to M82 is not covered by Auger.

Anisotropy

Telescope Array

[abb18]

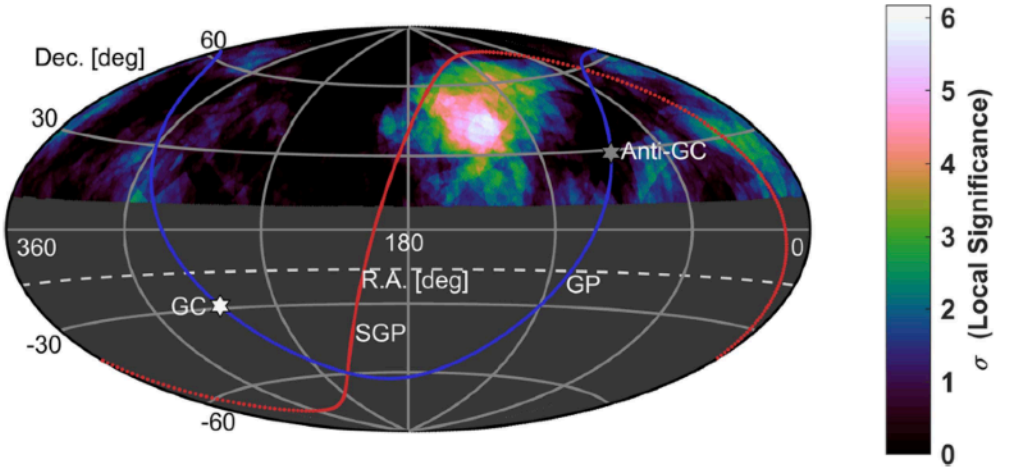

Figure 3. Projection of the energy spectrum anisotropy local pre-trial significance, for 14.03% equal exposure spherical cap bins ($E \geqslant 10^{19.2}$ eV). The maximum is $6.17\sigma_{\rm local}$ at $9^{\rm h}16^{\rm m}$, 45° and is 7° from the the Hotspot location of Abbasi et al. (2014a). The dashed curve at decl. $= -16°$ defines the FOV. Solid curves indicate the Galactic plane (GP) and supergalactic plane (SGP). White and gray hexagrams indicate the Galactic center (GC) and anti-galactic center (Anti-GC).

Anisotropy

Auger and TA

[anc19]

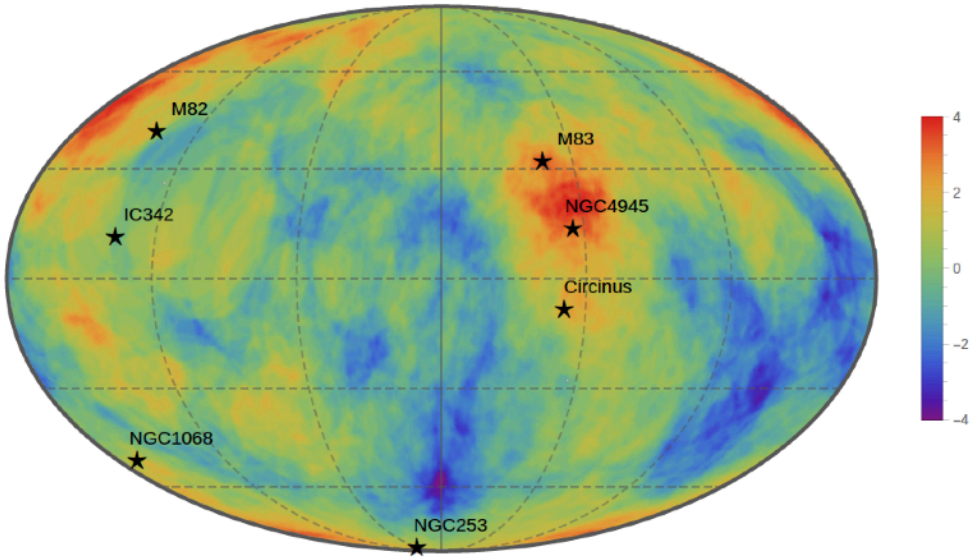

Figure 7: Skymap in Galactic coordinates of the Li-Ma significances of over-densities in 20° radius windows for 840 events recorded by Auger with $E > E_{\mathrm{th,Auger}}$ and 130 events recorded by TA with $E > E_{\mathrm{th,TA}}$. The color scale indicates the significance in units of standard deviations; negative values follow the convention of indicating the (positive) significance of deficits. Nearby SBGs providing a significant contribution to the UHECR correlation signal of Auger [3] and TA [163] are indicated by stars. From Ref. [161].

Auger data with a model prediction of deflection of UHECRs by galactic and extragalactic magnetic fields.

Again the composition of UHECRs is important.

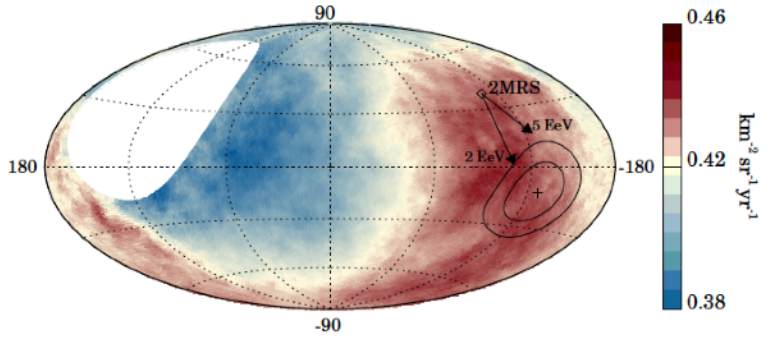

UHECR the Challenges

[ast19]

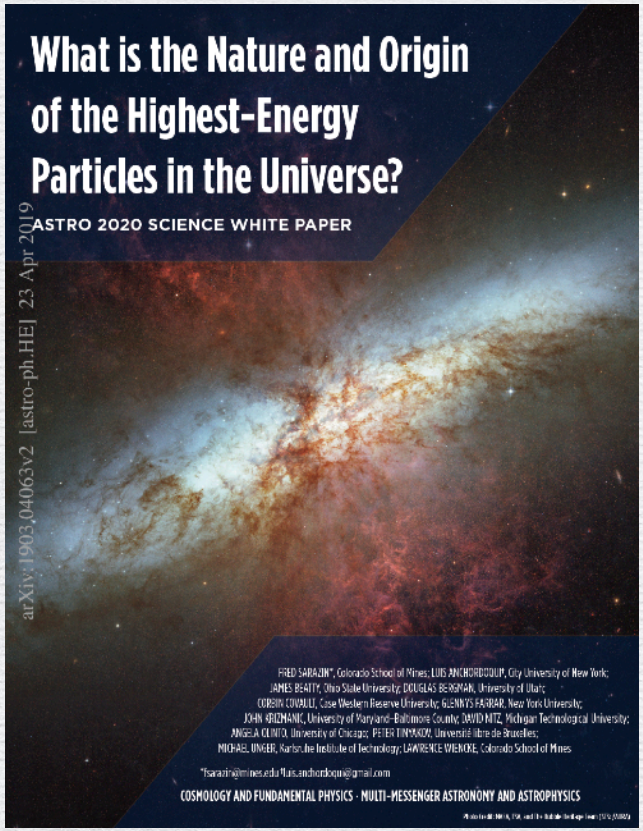

The big questions and goals for the next decade

tions: *What is the nature and origin of UHECRs? How are UHECRs accelerated to such extreme energies? Are there multiple types of sources and acceleration mechanisms? Do UHECRs consist of both protons and heavier nuclei, and how does the composition evolve as a function of energy?*

In order to address these questions, the goals for the next decade will be to: identify one or more nearby UHECR sources, refine the spectrum and composition of the highest-energy Galactic

The UHECR paradigm shift

and their sources. Prior to the development of very large, hybrid detectors, it was commonly believed that UHECRs were protons, that a spectral cutoff (if indeed there was one!) should be due to "GZK" energy losses on the cosmic microwave background [1, 2], that the Galactic-extragalactic transition would be marked by a shift from Galactic iron to extragalactic protons, and that the *ankle* feature at a few EeV marked the Galactic-extragalactic transition. We know now that this simple picture is mostly, if not entirely, wrong.

$\sqrt{s}_{pp}$ (TeV)

suggest a gradual increase of the average mass of cosmic rays with energy. Interpreting the data with LHC-tuned hadronic interaction models gives a mean baryon number $A \approx 14 - 20$ at $E \approx 10^{19.5}$ eV. The Auger-TA joint working group on composition concluded that the measurements of the average shower maximum by TA and Auger are compatible within experimental uncertainties at all energies [21, 22]. The observed decrease of the standard deviation of the $X_{\rm max}$ distributions

multi-messenger program. IceCube, Auger, and ANITA limits already challenge models in which the highest-energy UHECRs are proton-dominated [37–44]. Additionally, UHECR experiments

Identifying candidate sources for extreme accelerators

reduced; here Z is the charge of the UHECR in units of the proton charge. Further refinements in measuring the composition evolution and possible composition anisotropy are crucial to source inference.

Stepping up to the new challenges

The more complex picture that has emerged over the past decade presents a challenge to discovering UHECR sources and unraveling how UHECRs are accelerated – the holy grail of multi-messenger astrophysics for decades. Yet, after about a decade of operation, both Auger and TA

Composition-assisted anisotropy studies add new potential to identify individual UHECR sources. With a mixed composition, UHECRs can experience large deflections by Galactic and extragalactic magnetic fields, even at the highest energies. Composition-tagging allows the subset of events with highest rigidity and hence smallest deflections to be selected, to strongly enhance source identification both with UHECRs alone and in combination with neutral messengers

References:

reviews:

[anc19] L.A. Anchordoqui, Phys. Rep. **801**, 1(2019).

[mol18] S. Mollerach and E. Roulet, Prog. in Part. and Nucl. Phys. **98**, 85 (2018).

[daw17] B.R. Dawson, M. Fukushima and P. Sokolsky, Prog. Theor. Exp. Phys. 2017, 12A101.

articles:

[aab14] A. Aab et al., Phys. Rev. D **90**, 122006 (2014).

[aab15] A. Aab et al., Astrophys. J **804**, 15 (2015).

[aab18] A. Aab et al., Astrophys. J. Lett. **853**, L29 (2018).

[abb18] R.U. Abbasi et al., Astrophys. J. **862**, 91 (2018).

[abb19] R.U. Abbass et al., Phys. Rev. D **99**, 022002 (2019).

[abu12] T. Abu-Zayyad *et al.*, Nucl. Instrum. and Methods in Phys. Res. A **689**, 87 (2012).

[all12] D. Allard, Astropart. Phys. **39-40**, 33 (2012).

[ast19] ASTRO2020 Science White Paper, arXiv:1903.04063v2 [astro-ph.HE]

[aug04] Auger Collaboration, Nucl. Instrum. and Methods in Phys. Res. A **523**, 50 (2004).

[aug15] The Pierre Auger Collaboration, Nucl. Instrum. and Methods in Phys. Res. A **798**, 172 (2015)

[aug15b] The Pierre Auger Collaboration, arXiv1604.03637 [astro-ph.IM].

[aug17] The Pierre Auger Collaboration, Science **357**, 1266 (2017).

[gor18] D. Góra, Universe **2018**, 4, 128.

[gre66] K. Greisen, Phys. Rev. Lett. **16**, 748 (1966).

[kha05] E. Khan et al., Astropart. Phys. **23**, 191 (2005).

[ste99] F.W. Stecker and M.H. Salamon, Astrophys. J **512**, 521 (1999).

[tok11] H. Tokuno *et al* J. Phys. Conf. Ser. 293, 012035(2011).

[tok12] H. Tokuno *et al.*, Nucl. Instrum. and Methods in Phys. Res. A **676**, 54 (2012).

[zat66] G.T. Zatsepin and V.A. Kuzmin, JETP Lett. **4**, 78 (1966).

[PDG2018] Review of particle physics, particle data group, Phys Rev. D **98**, 1(2018).

Thank you

for your attention